# ADVANCEMENT OF ROTORDYNAMIC TOPICS

A Thesis

presented to

the Faculty of California Polytechnic State University,

San Luis Obispo

In Partial Fulfillment

of the Requirements for the Degree

Master of Science in Mechanical Engineering

by

Cameron Naugle

April 2018

COMMITTEE MEMBERSHIP

| | |
|---|---|
| TITLE: | Advancement of Rotordynamic topics |
| AUTHOR: | Cameron Naugle |
| DATE SUBMITTED: | April 2018 |
| COMMITTEE CHAIR: | Xi (Julia) Wu, Ph.D.<br>Professor of Mechanical Engineering |
| COMMITTEE MEMBER: | Mohammad Noori<br>Professor of Mechanical Engineering |
| COMMITTEE MEMBER: | Hemanth Porumamilla<br>Professor of Mechanical Engineering |
| COMMITTEE MEMBER: | Peter Schuster<br>Professor of Mechanical Engineering |

ABSTRACT

Advancement of Rotordynamic topics

Cameron Naugle

Your abstract goes in here

# ACKNOWLEDGMENTS

Thanks to:

-

TABLE OF CONTENTS

LIST OF TABLES

LIST OF FIGURES

Chapter 1

# FINITE ELEMENT METHOD FOR ROTORDYNAMIC SYSTEMS

## 1.1 Beam Element FE Equation

### 1.1.1 Bernoulli-Euler Beam equation

Assumptions used to derive the Bernoulli-Euler beam equation are (Complete derivation in [7]):

1. Beam is bending in a plane, in this case in the y-direction, where the x-direction is along the length of the beam.
2. The neutral axis undergoes no deformation in the longitudinal direction.
3. Cross sections remain plane and perpendicular to the nuetral axis.
4. The material is linear-elastic.
5. Stresses in the y and z direction are negligible compared to those in the x direction.
6. Rotary inertial effects are not considered.
7. Mass density is constant at each cross section, so that each mass center is coincident with the centroid of that section.

Using kinematics and assumptions 2 & 3, the strain in the x direction may be related to the curvature of the beam, $\mu(x,t)$, and the distance from the neutral axis by

$$\epsilon = -\frac{y}{\mu} \tag{1.1}$$

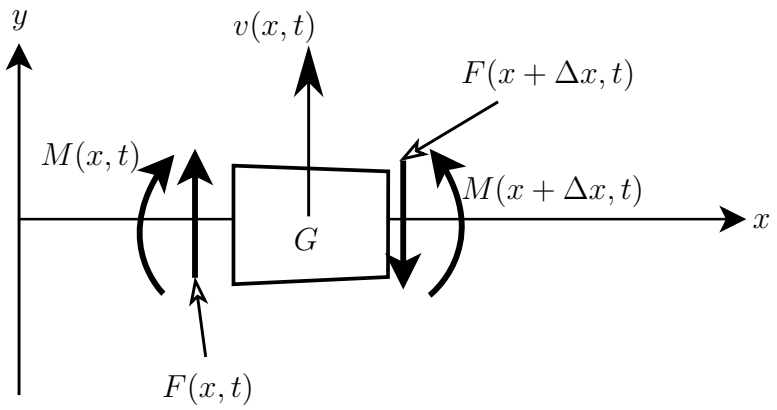


**Figure 1.1: Free body diagram of a beam section in planar bending.**

then, with assumption 4 & 7 the relation from curvature to moment is

$$M(x,t) = \frac{EI}{\mu} \tag{1.2}$$

where $E$, Young's modulus, and $I$, area moment of inertia are constant in cross sections. By using Newton's laws and the free body diagram of a single beam element, see Figure 1.1, the equations of motion are summarized as:

$$\sum F_y = \Delta m \ddot{v} \quad \& \quad \sum M_G = 0 \tag{1.3}$$

Moment equation is represented as moments summarized at the center of mass, $G$. The right hand side of moment equation of EOM (1.3) is know to be null due to assumption 6. Applying Newton's equations (1.3) to the FBD of Figure 1.1 results in the force equation

$$F(x,t) - F(x+\Delta x,t) = \rho A \Delta x \frac{\partial^2 v}{\partial t^2} \tag{1.4}$$

and moment equation

$$-M(x,t) + M(x+\Delta x,t) + F(x,t)\left(\frac{-\Delta x}{2}\right) + [-F(x+\Delta x,t)]\left(\frac{\Delta x}{2}\right) = 0 \tag{1.5}$$

Taking the limit of equations (1.4) & (1.5) as $\Delta x \to 0$ results in equations (1.6) & (1.7) respectively.

$$\frac{\partial F}{\partial x} = -\rho A \frac{\partial^2 v}{\partial t^2} \tag{1.6}$$

$$\frac{\partial M}{\partial x} - F = 0 \tag{1.7}$$

Assuming the beam slope, $\frac{\partial v}{\partial x}$, remains relatively small, then linearized curvature of the beam is inversely related to $\frac{\partial^2 v}{\partial x^2}$. Substituting this linearized curvature in (1.2) produces

$$M(x,t) = EI\frac{\partial^2 v}{\partial x^2} \tag{1.8}$$

Using linearized moment equation (1.8), combined with (1.6) & (1.7) lends the Euler beam equation

$$\frac{\partial^2}{\partial x^2}\left(EI\frac{\partial^2 v}{\partial x^2}\right) = -\rho A\frac{\partial^2 v}{\partial t^2} \tag{1.9}$$

This is the governing differential equation for transverse motion of a slender beam. This equation is not suitable for an application involving lengths that are not much greater than the width of the beam [16].

### 1.1.2 Timoshenko Beam Finite Element

The Timoshenko beam element allows for the beam cross section plane at any axis location to differ from normal with the axis of the beam. In other words, the element allows for shear stresses. This element often also includes the effects of rotary inertia and gyroscopic moments, as it will in this derivation. Generalized displacements used are assumed to be variable in both time and space. The element has six degrees of freedom. Three translation and three rotations all defined on the beam axis. So then all displacements are functions of time, $t$, and the axial spacial coordinate, $x$.

#### 1.1.2.1 Kinematic Relationships

In order to develop the stresses and strains internal to the beam, and subsequently the equations of motion, the motion of some arbitrary point on the beam must be defined in terms of the generalized coordinates. Motion of two points is taken into

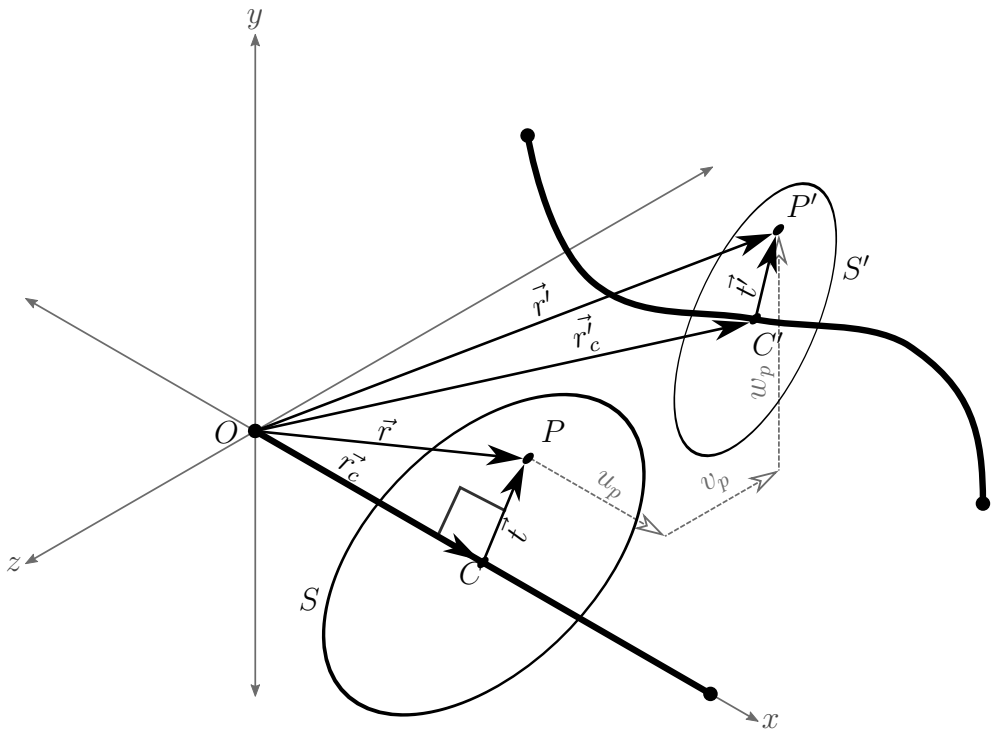


**Figure 1.2: Beam Element with nodal displacements.**

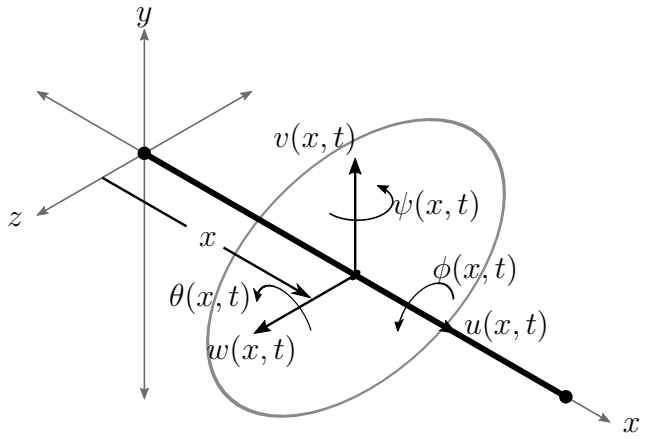


**Figure 1.3: Timoshenko beam section with degrees of freedom at some point x along beam axis.**

consideration to assist in dividing the motion into a translation and a rotation. These points are shown in Figure 1.2. The first point, $C$, falls on the beam axis at location x, and in the undeformed configuration, the vector $\vec{r}_c' = \overrightarrow{OC}$ forms a right angle with the surface of the cross section. The second point, $P$ is at some arbitrary $(y, z)$ location on the cross section. The vecor $\vec{t} = \overrightarrow{CP}$ points from the beam axis to the point along the cross section. If we follow this point $P$ we will be able to define the motion of the cross section as a whole, or more succinctly, to define the displacements $u_p, v_p, w_p$ in terms of the coordinates $u, v, w, \psi, \theta,$ & $\phi$. The motion of point P is split into translation and rotation, where $\vec{t}$ is rotated and $\vec{r}_c$ is translated to point to the deformed location $P'$. The vector pointing to P in the undeformed state is defined as

$$\vec{r} = \vec{r}_c + \vec{t} \tag{1.10}$$

Rotations are represented with a rotation transformation matrix,

$$\vec{t}' = \underline{R}\vec{t} \tag{1.11}$$

The linearized first order rotational matrix for small angles is represented by

$$\underline{R} = \begin{bmatrix} 1 & -\theta & \psi \\ \theta & 1 & -\phi \\ -\psi & \phi & 1 \end{bmatrix} \tag{1.12}$$

and the translation with a displacement vector

$$\vec{r}_c' = \vec{r}_c + \vec{u} \tag{1.13}$$

Combined motion from $P$ to $P'$ can be defined by

$$\vec{u}_p = \vec{r'} - \vec{r} \tag{1.14}$$

where $\vec{u}_p$ is the vector containing $u_p$, $v_p$, & $w_p$. The vector definitions for $\vec{r}'$ and $\vec{r}$ are substituted to the above equation to obtain

$$\vec{u}_p = \vec{r}_c' + \vec{t'} - \vec{r}_c + \vec{t} \tag{1.15}$$

and now using the definition for $\vec{u}$ and $\vec{t}$ leads to the simplified expression for the motion of $P$

$$\vec{u}_p = \vec{u} + (\underline{R} - \underline{I})\vec{t} \tag{1.16}$$

expanding matrices reveals the equation

$$\vec{u}_p = \begin{Bmatrix} u_p \\ v_p \\ w_p \end{Bmatrix} = \begin{Bmatrix} u \\ v \\ w \end{Bmatrix} + \begin{bmatrix} 0 & -\theta & \psi \\ \theta & 0 & -\phi \\ -\psi & \phi & 0 \end{bmatrix} \begin{Bmatrix} 0 \\ y \\ z \end{Bmatrix} \tag{1.17}$$

Therefore, the motion of any point on the beam may be approximated with

$$\vec{u}_p = \begin{Bmatrix} u - \theta y + \psi z \\ v - \phi z \\ w + \phi y \end{Bmatrix} \tag{1.18}$$

#### 1.1.2.2 Internal Constitutive Relationship

Stresses are assumed to exist in the beam in the axial direction, and in shear on the face of the beam section. Stresses in the transverse, or the y and z, directions are assumed negligible. Shear stresses out of the plane section are assumed to be vanishing as the differential element shrinks. Internal damping is to be considered independently from this material constitutive relationship. Written out, these stresses are represented by the matrix

$$\sigma_{ij} = \begin{bmatrix} \sigma_{xx} & \sigma_{xy} & \sigma_{xz} \\ \sigma_{xy} & 0 & 0 \\ \sigma_{xz} & 0 & 0 \end{bmatrix} \tag{1.19}$$

using the Hooke's Law for a linear elastic isotropic material, expressed as

$$\epsilon_{ij} = \frac{1}{E}[(1+\nu)\sigma_{ij} - \nu\delta_{ij}\sigma_{kk}] \tag{1.20}$$

allows the determination of the stress strain relationship in engineering notation as

$$\begin{Bmatrix} \sigma_{xx} \\ \sigma_{xy} \\ \sigma_{xz} \end{Bmatrix} = \begin{bmatrix} E & 0 & 0 \\ 0 & 2G & 0 \\ 0 & 0 & 2G \end{bmatrix} \begin{Bmatrix} \epsilon_{xx} \\ \epsilon_{xy} \\ \epsilon_{xz} \end{Bmatrix} \tag{1.21}$$

where, $G = \frac{E}{2(1+\nu)}$. Strains are derived from displacements of equation (1.18) using a linear strain-displacement relationship for infinitesimal strains: $2\epsilon_{ij} = u_{i,j} + u_{j,i}$.

$$\begin{cases} \epsilon_{xx} = u' - \theta' y + \psi' z \\ \epsilon_{xy} = \frac{1}{2}(v' - \phi' z - \theta) \\ \epsilon_{xz} = \frac{1}{2}(w' + \phi' y + \psi) \end{cases} \tag{1.22}$$

Note that in the case of the Euler-Bernoulli beam derivation the slope in a transverse direction displacement is equal to the rotation angle about the orthogonal transverse axis, i.e., $v' = \theta$ and $w' = \psi$. Application of those would reduce the system to the Euler-Bernoulli beam.

It will be proven useful to introduce generalized strains that group strain contributions above as axial, bending, torsion, and shear, represented by the symbols $\varepsilon$, $\rho$, $\varphi$, $\gamma$,respectively.

$$\begin{cases} \varepsilon = u' \\ \rho_y = -\theta' \\ \rho_z = \psi' \\ \varphi = \phi' \\ \gamma_y = v' - \theta \\ \gamma_z = w' + \psi \end{cases} \tag{1.23}$$

allowing the representation of the strains from eq (1.22) using the generalized strains as:

$$\begin{cases} \epsilon_{xx} = \varepsilon + \rho_y y + \rho_z z \\ \epsilon_{xy} = \frac{1}{2}(\gamma_y - \varphi z) \\ \epsilon_{xz} = \frac{1}{2}(\gamma_z + \varphi y) \end{cases} \tag{1.24}$$

Now the stresses in equation (1.21) can be represented with the displacements as

$$\left\{ \begin{array}{c} \sigma_{xx} \\ \sigma_{xy} \\ \sigma_{xz} \end{array} \right\} = \left\{ \begin{array}{c} E(u' - \theta' y + \psi' z) \\ G(v' - \phi' z - \theta) \\ G(w' + \phi' y + \psi) \end{array} \right\} = \left\{ \begin{array}{c} E(\varepsilon + \rho_y y + \rho_z z) \\ G(\gamma_y - \varphi z) \\ G(\gamma_z + \varphi y) \end{array} \right\} \tag{1.25}$$

$$U = \int_V \sigma_{ij} \epsilon_{ij} dV \tag{1.26}$$

Now the inner product of the total virtual strain energy can be expanded

$$U = \int_V \left[ \sigma_{xx} \epsilon_{xx} + 2\sigma_{xy} \epsilon_{xy} + 2\sigma_{xz} \epsilon_{xz} \right] dV \tag{1.27}$$

Then expand virtual strains into the generalized strains corresponding to the degrees of freedom of the beam element and collect terms on generalized strains

$$U = \int_V \left[ \sigma_{xx} \varepsilon + \sigma_{xx} y \rho_y + \sigma_{xx} z \rho_z + \sigma_{xy} \gamma_y + \sigma_{xz} \gamma_z + (\sigma_{xz} y - \sigma_{xy} z) \varphi \right] dV \tag{1.28}$$

this internal mechanical energy expression allows us to recognize stresses conjugate with each generalized strain as the corresponding stress for that phenomena. Integration allows the determination of the forces and moments related to each generalized strain as

$$\left\{ \begin{array}{lll} N = & \int_A \sigma_{xx} dA & = E(A\varepsilon + S_y \rho_y + S_z \rho_z) \\ M_y = & \int_A \sigma_{xx} z dA & = E(S_z \varepsilon + I_{xy} \rho_y + I_y \rho_z) \\ M_z = & \int_A \sigma_{xx} y dA & = E(S_y \varepsilon + I_z \rho_y + I_{xy} \rho_z) \\ Q_y = & \int_A \sigma_{xy} dA & = \kappa G(A\gamma_y - S_z \varphi) \\ Q_z = & \int_A \sigma_{xz} dA & = \kappa G(A\gamma_z + S_y \varphi) \\ M_x = & \int_A (\sigma_{xz} y - \sigma_{xy} z) dA & = \kappa G \left( A_y \gamma_z - A_z \gamma_y + J_x \varphi \right) \end{array} \right. \tag{1.29}$$

$$\text{where, } \left\{ \begin{array}{ll} \kappa = \frac{6(1+\nu)}{7+6\nu}, \textit{for circular cross sections.} & \\ A = \int_A dA & S_y = \int_A y dA \\ S_z = \int_A z dA & I_y = \int_A z^2 dA \\ I_z = \int_A y^2 dA & J_x = I_y + I_z \end{array} \right.$$

$\kappa$ is the shear coefficient which attempts to correct for the fact that the shear strain is not constant over the beam cross section. Assuming the central axis of the beam is coincident with the shear center, then $A_y = A_z = I_{xy} = 0$. Which simplifies the conjugate forces to

$$\begin{cases} N = EA\varepsilon & = EAu' \\ M_y = EI_y\rho_z & = EI_y\psi' \\ M_z = EI_z\rho_y & = -EI_z\theta' \\ Q_y = \kappa GA\gamma_y & = \kappa GA(v' - \theta) \\ Q_z = \kappa GA\gamma_z & = \kappa GA(w' + \psi) \\ M_x = \kappa GJ_x\varphi & = \kappa GJ_x\phi' \end{cases} \tag{1.30}$$

#### 1.1.2.3 Differential Equations of Motion

Now the equations are motion are derived for the Timoshenko beam element. External forces are not included in this derivation. Though they may easily be added to the diagram of figure 1.4 and included in the analysis. It is also assumed that the cross section remains planar during deformation and the material properties are homogeneous through time and space. The derivation is the same as for a Euler-Bernoulli beam with the exception of the constitutive relations used at the end and the inclusion of torsion and axial degrees of freedom. Using conservation of momentum and conservation of the moment of momentum a relationship between inertia and internal forces is developed. Applying summation of forces in the x-direction

$$(N + \frac{1}{2}\frac{\partial N}{\partial x}dx) - (N - \frac{1}{2}\frac{\partial N}{\partial x}dx) = \rho A dx \frac{\partial^2 u}{\partial x^2} \tag{1.31}$$

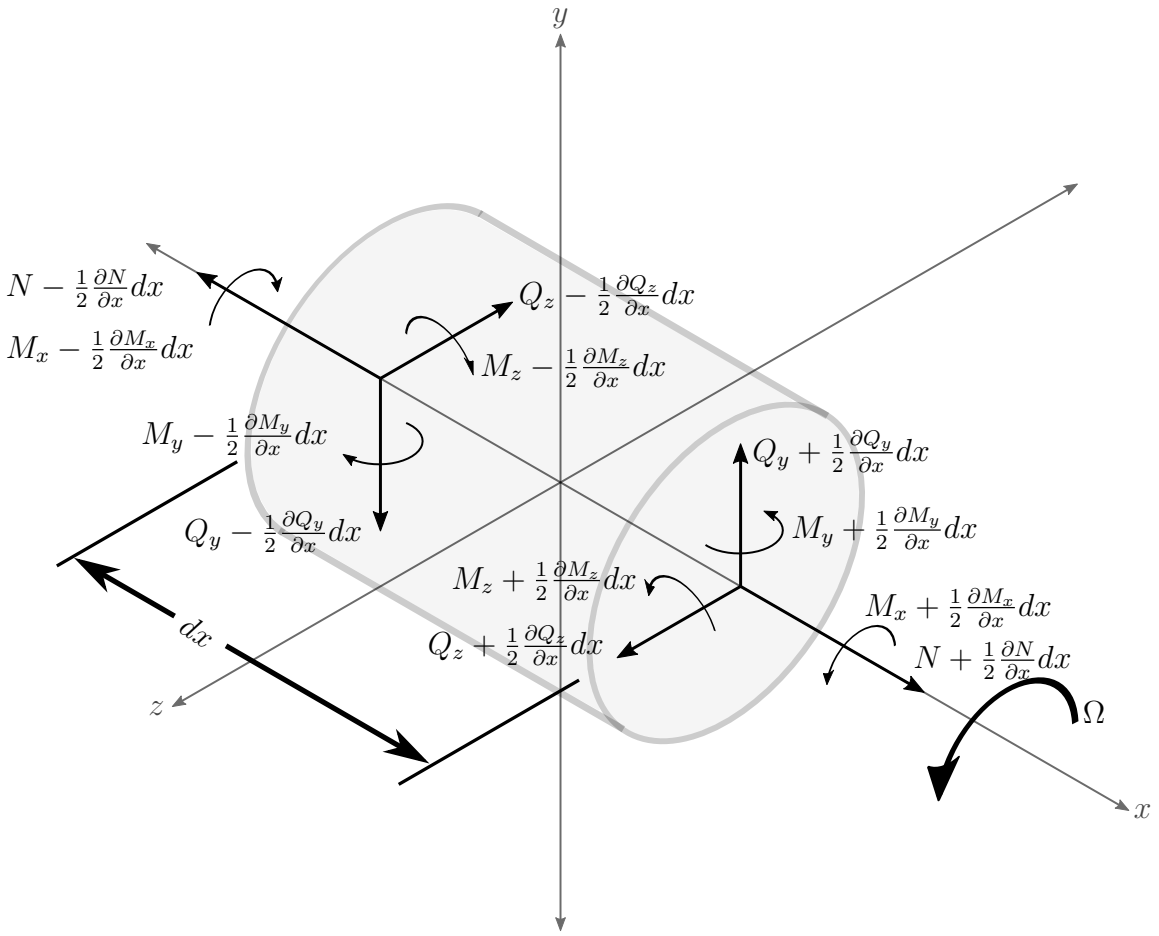


**Figure 1.4: Beam differential element with generalized forces.**

by Simplifying the above equation, and performing the same steps for the other directions and moments we get

$$\begin{cases} \frac{\partial N}{\partial x} = \rho A \frac{\partial^2 u}{\partial x^2} \\ \frac{\partial Q_y}{\partial x} = \rho A \frac{\partial^2 v}{\partial x^2} \\ \frac{\partial Q_z}{\partial x} = \rho A \frac{\partial^2 w}{\partial x^2} \\ \frac{\partial M_y}{\partial x} - Q_z = \rho I_y \frac{\partial^2 \psi}{\partial x^2} + \rho J_x \Omega \frac{\partial \theta}{\partial x} \\ \frac{\partial M_z}{\partial x} + Q_y = \rho I_z \frac{\partial^2 \theta}{\partial x^2} - \rho J_x \Omega \frac{\partial \psi}{\partial x} \\ \frac{\partial M_x}{\partial x} = \rho J_x \frac{\partial^2 \phi}{\partial x^2} \end{cases} \tag{1.32}$$

Gyroscopic moments have been explicitly added to the summations in the appropriate equations. The generalized forces of equation (1.30) are substituted in the equilibrium equations (1.32)

$$\begin{cases} EAu'' = \rho A \ddot{u} & \text{(1.33a)} \\ \kappa GA(v'' - \theta') = \rho A \ddot{v} & \text{(1.33b)} \\ \kappa GA(w'' + \psi') = \rho A \ddot{w} & \text{(1.33c)} \\ EI_y \psi'' - \kappa GA(w' + \psi) = \rho I_y \ddot{\psi} + \rho J_x \Omega \dot{\theta} & \text{(1.33d)} \\ EI_z \theta'' + \kappa GA(v' - \theta) = \rho I_z \ddot{\theta} - \rho J_x \Omega \dot{\psi} & \text{(1.33e)} \\ \kappa GJ_x \phi'' = \rho J_x \ddot{\phi} & \text{(1.33f)} \end{cases}$$

In matrix form, this system of equations can be represented by this equation

$$\underline{\mathcal{M}}^e \ddot{\vec{\mathbf{u}}} + \Omega \underline{\mathcal{G}}^e \dot{\vec{\mathbf{u}}} - \left( \frac{\partial()}{\partial x} \underline{\mathcal{S}}^e - \underline{\mathcal{P}}^e \underline{\mathcal{S}}^e \right) \vec{\mathbf{u}} = 0 \tag{1.34}$$

where,

$$\begin{cases} \underline{\mathcal{M}}^e = \begin{bmatrix} \rho A & 0 & 0 & 0 & 0 & 0 \\ 0 & \rho A & 0 & 0 & 0 & 0 \\ 0 & 0 & \rho I_y & 0 & 0 & 0 \\ 0 & 0 & 0 & \rho I_z & 0 & 0 \\ 0 & 0 & 0 & 0 & \rho A & 0 \\ 0 & 0 & 0 & 0 & 0 & \rho J_x \end{bmatrix} \quad \underline{\mathcal{G}}^e = \begin{bmatrix} 0 & 0 & 0 & 0 & 0 & 0 \\ 0 & 0 & 0 & 0 & 0 & 0 \\ 0 & 0 & 0 & \rho J_x & 0 & 0 \\ 0 & 0 & -\rho J_x & 0 & 0 & 0 \\ 0 & 0 & 0 & 0 & 0 & 0 \\ 0 & 0 & 0 & 0 & 0 & 0 \end{bmatrix} \\ \underline{\mathcal{P}}^e = \begin{bmatrix} 0 & 0 & 0 & 0 & 0 & 0 \\ 0 & 0 & 0 & 0 & 0 & 0 \\ 0 & 1 & 0 & 0 & 0 & 0 \\ -1 & 0 & 0 & 0 & 0 & 0 \\ 0 & 0 & 0 & 0 & 0 & 0 \\ 0 & 0 & 0 & 0 & 0 & 0 \end{bmatrix} \quad \underline{\mathcal{S}}^e = \begin{bmatrix} \kappa GA\frac{\partial()}{\partial x} & 0 & 0 & -\kappa GA & 0 & 0 \\ 0 & \kappa GA\frac{\partial()}{\partial x} & \kappa GA & 0 & 0 & 0 \\ 0 & 0 & EI_y\frac{\partial()}{\partial x} & 0 & 0 & 0 \\ 0 & 0 & 0 & EI_z\frac{\partial()}{\partial x} & 0 & 0 \\ 0 & 0 & 0 & 0 & EA\frac{\partial()}{\partial x} & 0 \\ 0 & 0 & 0 & 0 & 0 & \kappa GJ_x\frac{\partial()}{\partial x} \end{bmatrix} \end{cases} \tag{1.35}$$

and $\vec{\mathbf{u}} = [v, w, \psi, \theta, u, \phi]^\intercal$ The principle of virtual displacements is utilized on the equations of motion to obtain the weak for of the equations of motion and integrated over the length of the beam.

$$\int_0^l \delta\vec{\mathbf{u}}^\intercal \underline{\mathcal{M}}^e \ddot{\vec{\mathbf{u}}} dx + \int_0^l \delta\vec{\mathbf{u}}^\intercal \Omega \underline{\mathcal{G}}^e \dot{\vec{\mathbf{u}}} - \int_0^l \delta\vec{\mathbf{u}}^\intercal \frac{\partial()}{\partial x} \underline{\mathcal{S}}^e \vec{\mathbf{u}} dx + \int_0^l \delta\vec{\mathbf{u}}^\intercal \underline{\mathcal{P}} \underline{\mathcal{S}}^e \vec{\mathbf{u}} dx = 0 \tag{1.36}$$

integration by parts on the third term and replacing $\underline{\mathcal{S}}$ with $\underline{\mathcal{D}}^e\underline{\mathcal{B}}$, and making use of the Identity matrix, $\underline{\mathbf{I}}$ where $\frac{\partial()}{\partial x}\underline{\mathbf{I}}$ is interpreted here as if the partial was a scalar

$$\int_0^l \delta\vec{\mathbf{u}}^\intercal \underline{\mathcal{M}}^e \ddot{\vec{\mathbf{u}}} dx + \Omega \int_0^l \delta\vec{\mathbf{u}}^\intercal \underline{\mathcal{G}}^e \dot{\vec{\mathbf{u}}} + \int_0^l \delta\vec{\mathbf{u}}^\intercal \left( \frac{\partial()}{\partial x}\underline{\mathbf{I}} + \underline{\mathcal{P}} \right) \underline{\mathcal{D}}^e \underline{\mathcal{B}} \vec{\mathbf{u}} dx = 0 \tag{1.37}$$

$$\underline{\mathcal{D}}^e = \begin{bmatrix} \kappa GA & 0 & 0 & 0 & 0 & 0 \\ 0 & \kappa GA & 0 & 0 & 0 & 0 \\ 0 & 0 & EI_y & 0 & 0 & 0 \\ 0 & 0 & 0 & EI_z & 0 & 0 \\ 0 & 0 & 0 & 0 & EA & 0 \\ 0 & 0 & 0 & 0 & 0 & \kappa GJ_x \end{bmatrix} \quad \& \quad \underline{\mathcal{B}} = \begin{bmatrix} \frac{\partial()}{\partial x} & 0 & 0 & -1 & 0 & 0 \\ 0 & \frac{\partial()}{\partial x} & 1 & 0 & 0 & 0 \\ 0 & 0 & \frac{\partial()}{\partial x} & 0 & 0 & 0 \\ 0 & 0 & 0 & \frac{\partial()}{\partial x} & 0 & 0 \\ 0 & 0 & 0 & 0 & \frac{\partial()}{\partial x} & 0 \\ 0 & 0 & 0 & 0 & 0 & \frac{\partial()}{\partial x} \end{bmatrix} \tag{1.38}$$

Notice that $\frac{\partial()}{\partial x}\underline{I} + \underline{\mathcal{P}} = \underline{\mathcal{B}}^\intercal$ so the equation of motion becomes

$$\int_0^l \delta\vec{\mathbf{u}}^\intercal \underline{\mathcal{M}}^e \ddot{\vec{\mathbf{u}}} dx + \Omega \int_0^l \delta\vec{\mathbf{u}}^\intercal \underline{\mathcal{G}}^e \dot{\vec{\mathbf{u}}} + \int_0^l \delta\vec{\mathbf{u}}^\intercal \underline{\mathcal{B}}^\intercal \underline{\mathcal{D}}^e \underline{\mathcal{B}} \vec{\mathbf{u}} dx = 0 \tag{1.39}$$

$\underline{\mathcal{M}}^e$ is the inertia of the element, $\underline{\mathcal{G}}^e$ is the rotating inertia, $\underline{\mathcal{D}}^e$ is the material stress-strain relationship, and $\underline{\mathcal{B}}^e$ is the strain-displacement operator. The solution of this differential system motivates a separation of variables that will be discussed in the next section.

#### 1.1.2.4 Shape Functions

The displacements thus far have been assumed to be functions of both position and time. Now the total displacement is separated into functions that depend on time and functions that depend on position. This is a fundamental part of the discretization of the beam element, and the use the finite element method.

$$\begin{cases} \vec{\mathbf{u}}(x,t) &= \underline{\mathbf{N}}(x)\vec{\mathbf{q}}(t) \\ \dot{\vec{\mathbf{u}}}(x,t) &= \underline{\mathbf{N}}(x)\dot{\vec{\mathbf{q}}}(t) \\ \ddot{\vec{\mathbf{u}}}(x,t) &= \underline{\mathbf{N}}(x)\ddot{\vec{\mathbf{q}}}(t) \\ \delta\vec{\mathbf{u}}(x,t) &= \underline{\mathbf{N}}(x)\delta\vec{\mathbf{q}}(t) \end{cases} \tag{1.40}$$

where, $\vec{\mathbf{u}} = [v, w, -\psi, \theta, u, \phi]^\intercal$ & $\vec{\mathbf{q}} = [v_1, w_1, -\psi_1, \theta_1, v_2, w_2, -\psi_2, \theta_2, u_1, \phi_1, u_2, \phi_2]^\intercal$. This specfic order of $\vec{\mathbf{q}}$ is chosen with $u$ and $\phi$ at the end to ease the condensation of the axial and torsional degrees of freedom out of the system if their use is not necessary for the system of interest. $\psi$ angles are defined as negative to allow for the same stiffness matrix to define the motion in both planes, and more importantly, to allow for the use of the complex plane to simplify the problem. The shape functions $\underline{\mathbf{N}}(x)$ interpolate the displacements between the beam ends. These functions must must solve the static portion of the differential equations (1.33). These shape functions are chosen as a polynomials that satisfy the boundary nodal displacements and rotations at the ends of a beam element. These nodal degrees of freedom, depicted in Figure 1.5 are considered to be interpolated through the beam element by the shape functions. Interpolation functions chosen are listed in Equation (1.41). Axial displacement, $u$, and torsional rotation, $\phi$ are independent, so their shape functions are

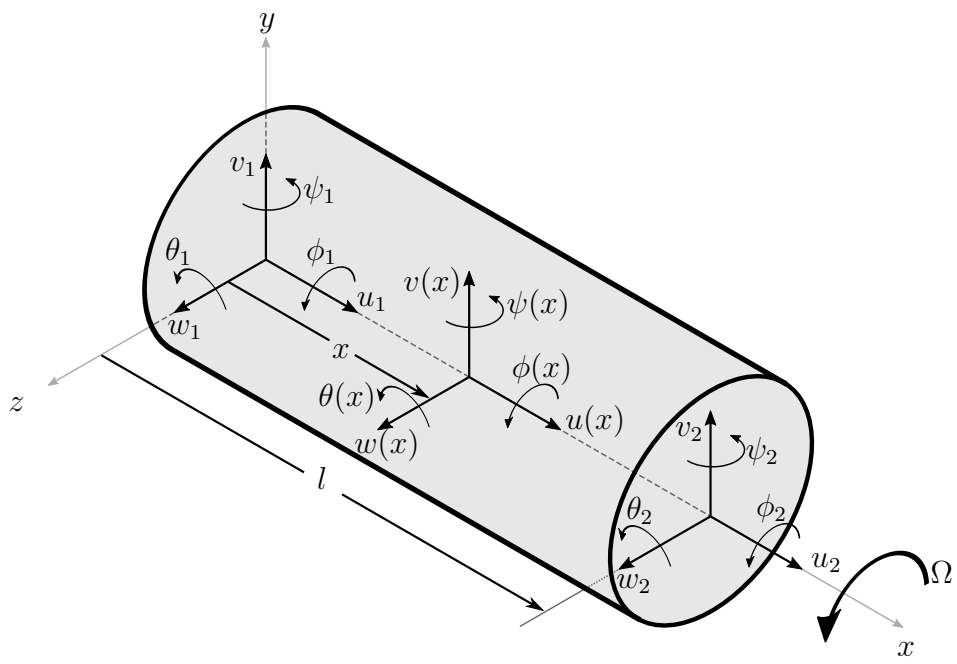


**Figure 1.5: Beam Element with nodal displacements.**

chosen as polynomials that satisfy the differential equation. Conversely, transverse displacements, $v$ & $w$, and bending rotations, $\psi$ & $\theta$ are coupled. Coupling of the shape functions has been proven to reduce some negative effects of linearly interpolated elements [25]. Polynomial functions are chosen for $v$ & $w$ and their rotational counterparts are derived using the differential relations.

$$\begin{cases} u = c_1 + c_2 x & \text{(1.41a)} \\ v = c_3 + c_4 x + c_5 x^2 + c_6 x^3 & \text{(1.41b)} \\ w = c_7 + c_8 x + c_9 x^2 + c_{10} x^3 & \text{(1.41c)} \\ \phi = c_{11} + c_{12} x & \text{(1.41d)} \end{cases}$$

$c_{1,2,\ldots}$ are the unknown constants of the polynomial solutions. Using transverse displacement of equations (1.41b) & (1.41c) in the differential equations (1.33b), (1.33c),

(1.33d), (1.33e) the interpolation functions of bending rotations are derived as:

$$\begin{cases} \psi = K_y c_{10} - c_8 - 2c_9 x - 3c_{10} x^2 & \text{(1.42a)} \\ \theta = K_z c_6 + c_4 + 2c_5 x + 3c_6 x^2 & \text{(1.42b)} \end{cases}$$

where, $K_y = \frac{6EI_y}{\kappa GA}$& $K_z = \frac{6EI_z}{\kappa GA}$ Boundary Conditions Boundary conditions for the interpolation polynomials of equations (1.41) & (1.42) are defined as the components of the vector $\vec{\mathbf{q}} u_j = u(x_j)$ and similarily for other degrees of freedom. Where, $j = 1, 2$ and defines the two states. In this derivation, $x_1 = 0$ and $x_2 = l$. Application of these boundary condition results in this relation between the polynomial constants and the boundary conditions.

$$\begin{Bmatrix} u_1 \\ u_2 \\ v_1 \\ v_2 \\ w_1 \\ w_2 \\ \psi_1 \\ \psi_2 \\ \theta_1 \\ \theta_2 \\ \phi_1 \\ \phi_2 \end{Bmatrix} = \begin{bmatrix} 1 & 0 & 0 & 0 & 0 & 0 & 0 & 0 & 0 & 0 & 0 & 0 \\ 1 & l & 0 & 0 & 0 & 0 & 0 & 0 & 0 & 0 & 0 & 0 \\ 0 & 0 & 1 & 0 & 0 & 0 & 0 & 0 & 0 & 0 & 0 & 0 \\ 0 & 0 & 1 & l & l^2 & l^3 & 0 & 0 & 0 & 0 & 0 & 0 \\ 0 & 0 & 0 & 0 & 0 & 0 & 1 & 0 & 0 & 0 & 0 & 0 \\ 0 & 0 & 0 & 0 & 0 & 0 & 1 & l & l^2 & l^3 & 0 & 0 \\ 0 & 0 & 0 & 0 & 0 & 0 & 0 & -1 & 0 & -K_y & 0 & 0 \\ 0 & 0 & 0 & 0 & 0 & 0 & 0 & -1 & -2l & -K_y - 3l^2 & 0 & 0 \\ 0 & 0 & 0 & 1 & 0 & K_z & 0 & 0 & 0 & 0 & 0 & 0 \\ 0 & 0 & 0 & 1 & 2l & K_z + 3l^2 & 0 & 0 & 0 & 0 & 0 & 0 \\ 0 & 0 & 0 & 0 & 0 & 0 & 0 & 0 & 0 & 0 & 1 & 0 \\ 0 & 0 & 0 & 0 & 0 & 0 & 0 & 0 & 0 & 0 & 1 & l \end{bmatrix} \begin{Bmatrix} c_1 \\ c_2 \\ c_3 \\ c_4 \\ c_5 \\ c_6 \\ c_7 \\ c_8 \\ c_9 \\ c_{10} \\ c_{11} \\ c_{12} \end{Bmatrix} \quad \text{(1.43)}$$

Inversion of this matrix results in a system of equations defining the constant $c_1$ through $c_{12}$. These constants are then substituted in to the polynomial expressions

(1.41) & (1.42) giving the interpolations as functions of the nodal displacements.

$$\begin{cases} u = N_1 u_1 + N_2 u_2 \\ v = T_{t_1 y} v_1 + T_{t_2 y} v_2 + T_{r_1 y} \theta_1 + T_{r_2 y} \theta_2 \\ w = T_{t_1 z} w_1 + T_{t_2 w} w_2 + T_{r_1 z} \psi_1 + T_{r_2 z} \psi_2 \\ \psi = R_{t_1 z} w_1 + R_{t_2 w} w_2 + R_{r_1 z} \psi_1 + R_{r_2 z} \psi_2 \\ \theta = R_{t_1 y} v_1 + R_{t_2 y} v_2 + R_{r_1 y} \theta_1 + R_{r_2 y} \theta_2 \\ \phi = N_1 \phi_1 + N_2 \phi_2 \end{cases} \tag{1.44}$$

with;

$$\begin{cases} N_1 = 1 - \zeta & N_2 = \zeta \\ T_{t_1 y,z} = \frac{1}{1+\alpha_{y,z}}(2\zeta^3 - 3\zeta^2 - \alpha_{y,z}\zeta + 1 + \alpha_{y,z}) & T_{t_2 y,z} = \frac{1}{1+\alpha_{y,z}}(-2\zeta^3 + 3\zeta^2 + \alpha_{y,z}\zeta) \\ T_{r_1 y,z} = \frac{l}{1+\alpha_{y,z}}[\zeta^3 - (2 + \frac{1}{2}\alpha_{y,z})\zeta^2 + (1 + \frac{1}{2}\alpha_{y,z})\zeta] & T_{r_2 y,z} = \frac{l}{1+\alpha_{y,z}}[\zeta^3 - (1 - \frac{1}{2}\alpha_{y,z})\zeta^2 - \frac{1}{2}\alpha_{y,z}\zeta] \\ R_{t_1 y,z} = \frac{6/l}{1+\alpha_{y,z}}(\zeta^2 - \zeta) & R_{t_2 y,z} = \frac{6/l}{1+\alpha_{y,z}}(-\zeta^2 + \zeta) \\ R_{r_1 y,z} = \frac{1}{1+\alpha_{y,z}}(3\zeta^2 - (4 + \alpha_{y,z})\zeta + 1 + \alpha_{y,z}) & R_{r_2 y,z} = \frac{1}{1+\alpha_{y,z}}(3\zeta^2 - (2 - \alpha_{y,z})\zeta) \end{cases} \tag{1.45}$$

where, $\alpha_y = 2K_y/l^2 = \frac{12EI_y}{\kappa GAl^2}$, $\alpha_z = 2K_z/l^2 = \frac{12EI_z}{\kappa GAl^2}$, & $\zeta = x/l$. (1.44) is expressed in matrix form as it appears in (1.40) where

$$\underline{\mathbf{N}}(x) = \begin{bmatrix} T_{t_1 y} & 0 & 0 & T_{r_1 y} & T_{t_2 y} & 0 & 0 & T_{r_2 y} & 0 & 0 & 0 & 0 \\ 0 & T_{t_1 z} & T_{r_1 z} & 0 & 0 & T_{t_2 z} & T_{r_2 z} & 0 & 0 & 0 & 0 & 0 \\ 0 & R_{t_1 z} & R_{r_1 z} & 0 & 0 & R_{t_2 z} & R_{r_2 z} & 0 & 0 & 0 & 0 & 0 \\ R_{t_1 y} & 0 & 0 & R_{r_1 y} & R_{t_2 y} & 0 & 0 & R_{r_2 y} & 0 & 0 & 0 & 0 \\ 0 & 0 & 0 & 0 & 0 & 0 & 0 & 0 & N_1 & 0 & N_2 & 0 \\ 0 & 0 & 0 & 0 & 0 & 0 & 0 & 0 & 0 & N_1 & 0 & N_2 \end{bmatrix} \tag{1.46}$$

still with the generalized displacement vector $\vec{\mathbf{q}} = [v_1, w_1, -\psi_1, \theta_1, v_2, w_2, -\psi_2, \theta_2, u_1, \phi_1, u_2, \phi_2]^{\intercal}$

Shape functions depend on the term $\alpha$ which is sometimes called the shear correction factor. This shear correction factor is proportional to the square of the ratio of radius to length of the beam element. So, as the length increases relative to the radius, $\alpha$ tends to zero. It will be evident in the following section that as $\alpha$ approaches

zero, the equations of motion approach the equations of the Bernoulli-Euler beam. A spatial representation of the shape functions of equation (1.45) is given in figure 1.6. Shape functions plotted with respect to the non-dimensional length lend a visu-

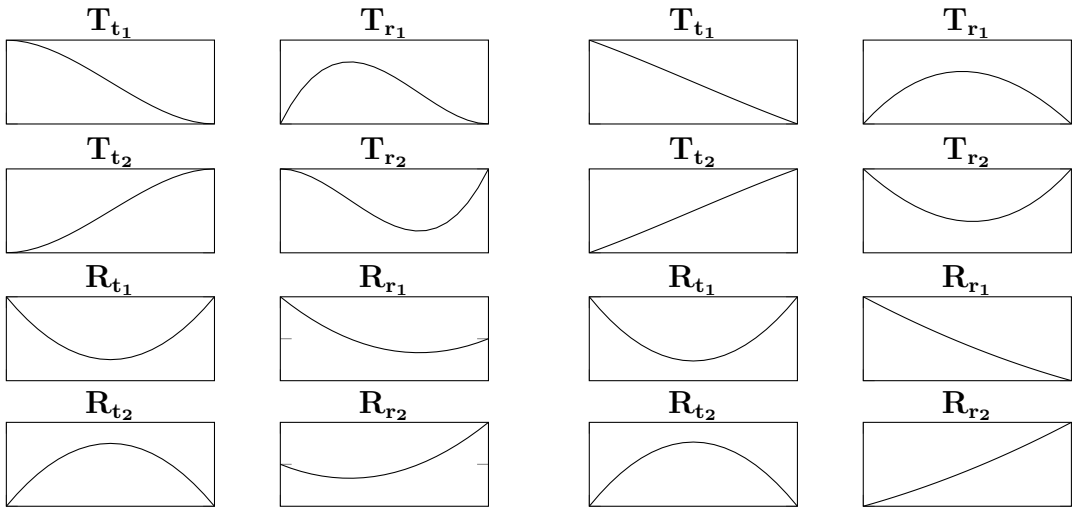


(a) length to radius ratio of 100. (b) length to radius ratio of 1.

**Figure 1.6: Shape Functions as they vary with $\zeta$ using two different ratios of length to radius of beam element.**

alization to the contribution of each shape function. Shape functions for axial and torsion are omitted since they are just linear polynomials. Each individual plot can be interpreted as a transformation from the input, being the coordinate multiplied to it, to the output of the variable function. For instance, the first shape function plot is the output of $v(x)$ with an input of $v_1$ while all other coordinates are zero. The shape makes sense under this interpretation, as the translation starts at some value, $v_1$ and decreases to zero at the end since $v_2$ is zero. Also, the expected shape breaks as the radius approaches the length as in Figure 1.6b. All shapes this beam will make in the model is a linear combination of the shapes shown here.

#### 1.1.2.5 Finite Equations of Motion

To obtain the equations of motion in terms of the generalized coordinates, $\vec{\mathbf{q}}$, displacement variables $\vec{\mathbf{u}}$ are replaced with definitions in equation 1.40.

$$\int_0^l \underline{\mathbf{N}}^{\intercal}\delta\vec{\mathbf{q}}^{\intercal}\underline{\mathcal{M}}^e\underline{\mathbf{N}}\ddot{\vec{\mathbf{q}}}dx + \Omega\int_0^l \underline{\mathbf{N}}^{\intercal}\delta\vec{\mathbf{q}}^{\intercal}\underline{\mathcal{G}}^e\underline{\mathbf{N}}\dot{\vec{\mathbf{q}}}dx + \int_0^l \underline{\mathbf{N}}^{\intercal}\delta\vec{\mathbf{q}}^{\intercal}\underline{\mathcal{B}}^{\intercal}\underline{\mathcal{D}}^e\underline{\mathcal{B}}\underline{\mathbf{N}}\vec{\mathbf{q}}dx = 0 \tag{1.47}$$

Note that $\vec{\mathbf{q}}$ is not dependent on x so it, and it's derivatives, may be pulled out of the integrals. Define $\underline{\mathbf{B}} = \underline{\mathcal{B}}\underline{\mathbf{N}}$ and substitute in, noting that $\underline{\mathbf{B}}$ interpolates strains from discrete displacements $\vec{\mathbf{q}}$. The motion equations are then

$$\int_0^l \underline{\mathbf{N}}^{\intercal}\underline{\mathcal{M}}^e\underline{\mathbf{N}}dx\ddot{\vec{\mathbf{q}}} + \Omega\int_0^l \underline{\mathbf{N}}^{\intercal}\underline{\mathcal{G}}^e\underline{\mathbf{N}}dx\dot{\vec{\mathbf{q}}} + \int_0^l \underline{\mathbf{B}}^{\intercal}\underline{\mathcal{D}}^e\underline{\mathbf{B}}dx\vec{\mathbf{q}} = 0 \tag{1.48}$$

Define

$$\begin{cases} \underline{\mathbf{M}}^e = \displaystyle\int_0^l \underline{\mathbf{N}}^{\intercal}\underline{\mathcal{M}}^e\underline{\mathbf{N}}dx & \text{(1.49a)} \\ \underline{\mathbf{G}}^e = \displaystyle\int_0^l \underline{\mathbf{N}}^{\intercal}\underline{\mathcal{G}}^e\underline{\mathbf{N}}dx & \text{(1.49b)} \\ \underline{\mathbf{K}}^e = \displaystyle\int_0^l \underline{\mathbf{B}}^{\intercal}\underline{\mathcal{D}}^e\underline{\mathbf{B}}dx & \text{(1.49c)} \end{cases}$$

so that, the general equations of motion for the timoshenko beam element are

$$\underline{\mathbf{M}}^e\ddot{\vec{\mathbf{q}}} + \Omega\underline{\mathbf{G}}^e\dot{\vec{\mathbf{q}}} + \underline{\mathbf{K}}^e\vec{\mathbf{q}} = 0 \tag{1.50}$$

Notwithstanding the inclusion of viscous and hysteretic internal damping phenomena. Derivations, and inclusion of these phenomena in the equations of motion are to be included in the following section.

#### 1.1.2.6 Rotating Internal Damping

Rotating damping is the main cause of instability in rotating machines. Non-rotating damping, such as the damping contributions from bearing supports, introduce a stabilizing effect. But, as rotating damping is dependent on rotation, its direction of force

can contribute to destabilization. Typically, friction components such as bearings with shrink fits or oil bearings are responsible for this destabilizing force. Due to the inherent complexity of modeling loose bearing components, or shrink fit dynamics, the analysis of the internal damping in the shaft elements is considered alone. This will allow for the study of the destabilizing effect in general, and the factors that may contribute stability such as structural damping and anisotropy of supports. Another area of interest is the design of components for specific rotor geometry to maximize the stability in the system. This stability analysis is only possible with the inclusion of some destabilizing force, [16],[15],[22],[36].

To motivate understanding of this force a simple derivation is provided with a rotating damping whose force is proportional to the flex of rate of change of the flex of the shaft. Obviously this is easier to define in the rotating reference frame, as the variables in this coordinate system directly represent the flex of the shaft from its neutral position. This relationship is as follows:

$$\vec{\mathcal{F}}_{\xi\eta} = -c_r \begin{Bmatrix} \dot{\xi}_c \\ \dot{\eta}_c \end{Bmatrix} \tag{1.51}$$

Now to translate this force back to the stationary reference frame, we will see the rotation transformation matrix

$$\underline{\mathcal{R}} = \begin{bmatrix} \cos\Omega t & \sin\Omega t \\ -\sin\Omega t & \cos\Omega t \end{bmatrix} \tag{1.52}$$

transforms stationary into rotating coordinates

$$\begin{cases} \begin{Bmatrix} \xi_c \\ \eta_c \end{Bmatrix} = \underline{\mathcal{R}} \begin{Bmatrix} y_c \\ z_c \end{Bmatrix} \\ \begin{Bmatrix} \dot{\xi}_c \\ \dot{\eta}_c \end{Bmatrix} = \underline{\mathcal{R}} \begin{Bmatrix} \dot{y}_c \\ \dot{z}_c \end{Bmatrix} + \dot{\underline{\mathcal{R}}} \begin{Bmatrix} y_c \\ z_c \end{Bmatrix} \end{cases} \tag{1.53}$$

where,

$$\underline{\dot{\mathcal{R}}} = \Omega \begin{bmatrix} -\sin\Omega t & \cos\Omega t \\ -\cos\Omega t & -\sin\Omega t \end{bmatrix} \tag{1.54}$$

substituting the second equation in 1.53 for the velocities in 1.51

$$\vec{\mathcal{F}}_{xy} = -c_r \begin{Bmatrix} \dot{y}_c \\ \dot{z}_c \end{Bmatrix} - c_r\Omega \begin{bmatrix} 0 & 1 \\ -1 & 0 \end{bmatrix} \begin{Bmatrix} y_c \\ z_c \end{Bmatrix} \tag{1.55}$$

From the equation (1.55) we see a dependence on both velocity and position. The portion dependent on the velocity is inherently stable as pulls opposite the motion. Conversely, the portion dependent on position cross couples the two displacements. This causes a destabilizing effect that grows as $\Omega$ increases. A net destabilizing force is produced once the latter portion of the exceeds the former. Without the presence of other structural damping forces, the system will destabilize.

For the beam element, the constitutive relationship[36] is comprised of both viscous and hysteretic forms of damping, $\eta_v$ & $\eta_h$ respectively.

$$\sigma_{xx} = E\left\{ \frac{\epsilon_{xx}}{\sqrt{1+\eta_h^2}} + \left( \eta_v + \frac{\eta_h}{\omega\sqrt{1+\eta_h^2}} \right) \dot{\epsilon}_{xx} \right\} \tag{1.56}$$

through the use of kinematics to obtain strain-displacement relations,

$$\begin{cases} \epsilon_{xx} &= -r\cos(\Omega-\omega)\, t\frac{\partial^2 R}{\partial x^2} \\ \dot{\epsilon}_{xx} &= (\Omega-\omega) r\sin(\Omega-\omega) t\frac{\partial^2 R}{\partial x^2} - r\cos(\Omega-\omega) t\frac{\partial}{\partial t}\frac{\partial^2 R}{\partial x^2} \end{cases} \tag{1.57}$$

and inspection to obtain moment equations,

$$\begin{cases} M_y &= \int_0^{2\pi}\int_0^a [w + r\sin\Omega t]\sigma_{xx} dr(rd(\Omega t)) \\ M_z &= \int_0^{2\pi}\int_0^a -[v + r\cos\Omega t]\sigma_{xx} dr(rd(\Omega t)) \end{cases} \tag{1.58}$$

we can complete a moment bending relationship to be used in the equations of motion

$$\begin{Bmatrix} M_y \\ M_z \end{Bmatrix} = EI \begin{bmatrix} \eta_a & \Omega\eta_v + \eta_b \\ \Omega\eta_v + \eta_b & -\eta_a \end{bmatrix} \begin{Bmatrix} v'' \\ w'' \end{Bmatrix} + EI \begin{bmatrix} \eta_v & 0 \\ 0 & -\eta_v \end{bmatrix} \begin{Bmatrix} \dot{v}'' \\ \dot{w}'' \end{Bmatrix} \tag{1.59}$$

where, $\eta_a = \frac{1+\eta_h}{\sqrt{1+\eta_h^2}}$ & $\eta_b = \frac{\eta_h}{\sqrt{1+\eta_h^2}}$

Now use the same strategy followed when solving for the weak form of the beam differential equations using the Principle of Virtual Displacements starting at equation (1.36). Then use the seperation of variables of defined by equation (1.40) to arrive at the total beam element equations of motion including internal damping as

$$\underline{\mathbf{M}}^e\ddot{\vec{\mathbf{q}}} + (\eta_v\underline{\mathbf{K}}^e + \Omega\underline{\mathbf{G}}^e)\dot{\vec{\mathbf{q}}} + [\eta_a\underline{\mathbf{K}}^e + (\Omega\eta_v + \eta_b)\underline{\mathbf{C}}^e]\vec{\mathbf{q}} = 0 \tag{1.60}$$

where,

$$\underline{\mathcal{I}} = \begin{bmatrix} 0 & 1 & 0 & 0 & 0 & 0 \\ -1 & 0 & 0 & 0 & 0 & 0 \\ 0 & 0 & 0 & 1 & 0 & 0 \\ 0 & 0 & -1 & 0 & 0 & 0 \\ 0 & 0 & 0 & 0 & 0 & 0 \\ 0 & 0 & 0 & 0 & 0 & 0 \end{bmatrix} \quad \& \quad \underline{\mathbf{C}}^e = \int_0^l \underline{\mathbf{B}}^\intercal\underline{\mathcal{I}}\underline{\mathcal{D}}\underline{\mathbf{B}}dx \tag{1.61}$$

$\underline{\mathbf{C}}^e$ is the "Circulation matrix", or the skew symmetric stiffness matrix.

#### 1.1.2.7 Beam Element in Complex Coordinates

Complex coordinates collapse the equations of each plane into one set of equations. This lends properties to a axisymmetric rotor systems that will be exploited in the analysis of the model. For the complex analysis in this body of work, the system is assumed to be axisymmetric and the torsional and axial degrees of freedom are omitted. Since the contributions from axial and torsional degrees of freedom are uncoupled from the system, there condensation has no effect on the remainder of system matrices. Complex coordinates used here are defined as:

$$\vec{\mathbf{s}} = \begin{Bmatrix} \vec{r} \\ \vec{p} \end{Bmatrix} = \begin{Bmatrix} v + iw \\ \theta - i\psi \end{Bmatrix} \tag{1.62}$$

Because the element is axisymmetric, and the special form of coordinates is used, symmetric beam equations in one plane hold for the complex plane and skew symmetric matrices become complex versions of the same matrix. Elemental matrices

can be formed using the collapsed version of the shape functions matrix

$$\underline{\mathbf{N}}^c = \begin{bmatrix} T_{t_1 y} & T_{r_1 y} & T_{t_2 y} & T_{r_2 y} \\ R_{t_1} & R_{r_1} & R_{t_2} & R_{r_2} \end{bmatrix} \tag{1.63}$$

in

$$\vec{\mathbf{s}} = \underline{\mathbf{N}}^c \vec{\mathbf{q}}^c \tag{1.64}$$

where $\vec{\mathbf{q}}^c = [\vec{\mathbf{s}}_1, \vec{\mathbf{s}}_2]^\intercal$.

To convince this property of the system in the complex plane, a proof for the elemental equations of motion will be made. Taking equation (1.33b), adding equation (1.33c) multiplied by the imaginary unit $i$ and using the definition for complex variables $\vec{p}$ and $\vec{r}$ leads to the transverse equation of motion in the complex plane

$$\kappa GA(\vec{r}'' - \vec{p}') = \rho A \ddot{\vec{r}} \tag{1.65}$$

and taking equation (1.33e) and subtracting equation (1.33d) multiplied by $i$ gives the rotation equation in the complex plane

$$EI\vec{p}'' - \kappa GA(\vec{r}' - \vec{p}) = \rho I \ddot{\vec{p}} + i\rho J\Omega\dot{\vec{p}} \tag{1.66}$$

which by inspection of both of these equations it is evident that the form is the same as equations (1.33b) and (1.33e) except for the imaginary unit on the cross coupled parts of the equation. Now that this idea is motivated, the finite element equations of motion analogous to equation (1.60) are

$$\underline{\mathbf{M}}^{ec}\ddot{\vec{\mathbf{q}}}^c + (\eta_v \underline{\mathbf{K}}^{ec} - i\Omega \underline{\mathbf{G}}^{ec})\dot{\vec{\mathbf{q}}}^c + [\eta_a \underline{\mathbf{K}}^{ec} - i(\Omega\eta_v + \eta_b)\underline{\mathbf{C}}^{ec}]\vec{\mathbf{q}}^c = 0 \tag{1.67}$$

## 1.2 Disk Nodal Equations

Since the beam element has been discretized into nodal degrees of freedom, so long as the locations of disks in the model are chosen to coincide with one of these nodal locations, the expressions for stiffness and inertia can be directly combined with the

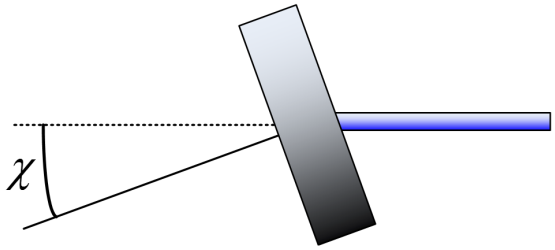


**Figure 1.7: Depiction of skew angle $\chi$**

global matrices at that node. The mass element is considered as a body at a point with inertia, gyroscopic moments, and unbalance considered as external forces.

$$\underline{\mathbf{M}}^d\ddot{\vec{\mathbf{q}}}_k + \Omega\underline{\mathbf{G}}^d\dot{\vec{\mathbf{q}}}_k = \Omega^2\vec{\mathbf{F}}^d \tag{1.68}$$

the superscript $d$ represents that the matrix or array is for a disk, and the subscript $_k$ on the displacement array indicates the array is only displacements for a single node, written out as: $\vec{\mathbf{q}}_k = [v, w, -\psi, \theta, u, \phi]^\intercal$. The matrices and forcing array of (1.68) are as follows,

$$\begin{cases} \underline{\mathbf{M}}^d = \begin{bmatrix} \rho Al & 0 & 0 & 0 & 0 & 0 \\ 0 & \rho Al & 0 & 0 & 0 & 0 \\ 0 & 0 & \rho I_z & 0 & 0 & 0 \\ 0 & 0 & 0 & \rho I_y & 0 & 0 \\ 0 & 0 & 0 & 0 & \rho Al & 0 \\ 0 & 0 & 0 & 0 & 0 & \rho J_x \end{bmatrix} \underline{\mathbf{G}} = \begin{bmatrix} 0 & 0 & 0 & 0 & 0 & 0 \\ 0 & 0 & 0 & 0 & 0 & 0 \\ 0 & 0 & 0 & \rho J_x & 0 & 0 \\ 0 & 0 & -\rho J_x & 0 & 0 & 0 \\ 0 & 0 & 0 & 0 & 0 & 0 \\ 0 & 0 & 0 & 0 & 0 & 0 \end{bmatrix} \\ \vec{\mathbf{F}}^d = \begin{Bmatrix} \rho Al\epsilon\cos(\Omega t + \delta_\varepsilon) \\ \rho Al\epsilon\sin(\Omega t + \delta_\varepsilon) \\ -\rho(I_y - J_x)\chi\sin(\Omega t) \\ \rho(I_z - J_x)\chi\cos(\Omega t) \\ 0 \\ 0 \end{Bmatrix} \end{cases} \tag{1.69}$$

Disk unbalance is caused by an eccentricity, or a geometrical distance between the axis of rotation and the center of mass of the disk. Eccentricity is represented here

as $\epsilon$ and is equivalent to that geometric distance. The moment unbalance forces, the third and fourth equations of $\vec{\mathbf{F}}^d$ in (1.69), are caused by the skew angle, $\chi$, which is the angle the disk major axis forms with the axis of rotation as in Figure 1.7. The major axis is the axis normal from the disk face from which the polar moment of inertia, $J_x$ is defined.

### 1.2.1 Disk in complex coordinates

Disk equations of motion (1.68) are converted to the complex plane in the same manner the beam element was derived in §1.1.2.7

$$\underline{\mathbf{M}}^{dc}\ddot{\vec{\mathbf{q}}}_k^c - i\Omega\underline{\mathbf{G}}^{dc}\dot{\vec{\mathbf{q}}}_k^c = \Omega^2\vec{\mathbf{F}}^{dc} \tag{1.70}$$

where,

$$\underline{\mathbf{M}}^{dc} = \begin{bmatrix} \rho Al & 0 \\ 0 & \rho I \end{bmatrix}, \quad \underline{\mathbf{G}}^{dc} = \begin{bmatrix} 0 & 0 \\ 0 & \rho J_x \end{bmatrix}, \quad \vec{\mathbf{F}}^{dc} = \begin{Bmatrix} \rho Al\epsilon e^{i\delta_\epsilon} e^{i\Omega t} \\ \rho(I - J_x)\chi e^{i\Omega t} \end{Bmatrix}$$

## 1.3 Bearing Nodal Equations

Bearings in this work are to be considered massless points of stiffness and damping acting at a node. Represented by the local equations of motion

$$\underline{\mathbf{D}}^b\dot{\vec{\mathbf{q}}}_k + \underline{\mathbf{K}}^b\vec{\mathbf{q}}_k = 0 \tag{1.71}$$

The superscript $^b$ indicates the matrix is for a bearing. A simple model for the stiffness and damping is used. Structural damping of the bearing is considered to be proportional to the stiffness, Raleigh Damping for the local bearing system. The

stiffness matrix is comprised of only transverse stiffness terms, as

$$\underline{\mathbf{K}}^b = \begin{bmatrix} k_{yy} & k_{yz} & 0 & 0 & 0 & 0 \\ k_{zy} & k_{zz} & 0 & 0 & 0 & 0 \\ 0 & 0 & 0 & 0 & 0 & 0 \\ 0 & 0 & 0 & 0 & 0 & 0 \\ 0 & 0 & 0 & 0 & 0 & 0 \\ 0 & 0 & 0 & 0 & 0 & 0 \end{bmatrix} \quad \underline{\mathbf{D}}^b = a\underline{\mathbf{K}}^b \tag{1.72}$$

The stiffness is typically simplified further to represent an orthotropic bearing, where $k_{yz} = k_{zy} = 0$ or further yet as a isotropic bearing, where $k_{yz} = k_{zy} = 0$ & $k_{yy} = k_{zz} = k$. Generally, these unknown parameters of stiffness are determined by changing the values to achieve the correct natural frequencies of the system.

### 1.3.1 Bearing in Complex Coordinates

Following the same methodology as sections §1.1.2.7 & §1.2.1, the equation of motion in the complex plane is

$$\underline{\mathbf{D}}^{bc}\dot{\vec{\mathbf{q}}}_k^c + \underline{\mathbf{K}}^{bc}\vec{\mathbf{q}}_k^c = 0 \tag{1.73}$$

where,

$$\underline{\mathbf{K}}^{bc} = \begin{bmatrix} k & 0 \\ 0 & k \end{bmatrix}, \quad \underline{\mathbf{D}}^{bc} = a\underline{\mathbf{K}}^{bc}$$

$k$ is the isotropic bearing stiffness. It is possible to define the complex system with anisotropic terms of stiffness, but the complexity added to the system outweighs the benefit of using the complex plane in the first place.

## 1.4 Assembly of the Global Systems of Equations

The matrices in the global system of equations are determined using the direct approach of taking the summation of the inertia, damping, stiffness, or force at each degree of freedom.

### 1.4.1 In the Real Coordinate System

$$\underline{\mathbf{M}}\ddot{\vec{\mathbf{q}}} + \underline{\mathbf{G}}\dot{\vec{\mathbf{q}}} + \underline{\mathbf{K}}\vec{\mathbf{q}} = \Omega^2\vec{\mathbf{F}} \tag{1.74}$$

Each summation is defined as

$$\begin{cases} \underline{\mathbf{M}} &= \underline{\mathbf{M}}_G^e + \underline{\mathbf{M}}_G^b + \underline{\mathbf{M}}_G^d & \underline{\mathbf{D}} &= \eta_v\underline{\mathbf{K}}_G^e + \Omega\underline{\mathbf{G}}_G^e + \Omega\underline{\mathbf{G}}_G^d + \underline{\mathbf{D}}_G^b \\ \underline{\mathbf{K}} &= \eta_a\underline{\mathbf{K}}_G^e + (\Omega\eta_v + \eta_b)\underline{\mathbf{C}}_G^e + \underline{\mathbf{K}}_G^b & \vec{\mathbf{F}} &= \vec{\mathbf{F}}_G^d \end{cases}$$

Subscript $_G$ indicates the matrix is in the global coordinate system that contains all of the degrees of freedom. Care must be taken here to associate the correct degrees of freedom, and recognize that some of the matrices are elemental and others are nodal.

### 1.4.2 In the Complex Coordinate System

$$\underline{\mathbf{M}}\ddot{\vec{\mathbf{q}}}^c + \underline{\mathbf{D}}\dot{\vec{\mathbf{q}}}^c + \underline{\mathbf{K}}\vec{\mathbf{q}}^c = \Omega^2\vec{\mathbf{F}} \tag{1.75}$$

where,

$$\begin{cases} \underline{\mathbf{M}} &= \underline{\mathbf{M}}_G^{ec} + \underline{\mathbf{M}}_G^{dc} + \underline{\mathbf{M}}_G^{bc} & \underline{\mathbf{D}} &= \eta_v\underline{\mathbf{K}}_G^{ec} - i\Omega(\underline{\mathbf{G}}_G^{ec} + \underline{\mathbf{G}}_G^{dc}) + \underline{\mathbf{D}}_G^{bc} \\ \underline{\mathbf{K}} &= \eta_a\underline{\mathbf{K}}_G^{ec} - i(\Omega\eta_v + \eta_b)\underline{\mathbf{C}}_G^{ec} + \underline{\mathbf{K}}_G^{bc} & \vec{\mathbf{F}} &= \vec{\mathbf{F}}_G^{dc} \end{cases}$$

### 1.4.3 Code Implementation

### 1.4.4 Model Reduction

#### 1.4.4.1 Static Condensation

## 1.5 Model Analysis

The benefit of the finite element model is the general linear ordinary differential equation that is left to solve in equations (1.74), & (1.75). Many techniques exist to provide frequency and time domain information on the solution to this system of equations. In rotordynamic analysis many of the analyses are interested in the

**Table 1.1: Properties of disks, shaft elements, and bearings of the example problem.**

| | $\rho[\frac{kg}{m^3}]$ | $r[m]$ | $\nu$ | $E[Pa]$ | $\eta_v[s]$ | $\eta_h$ |
|---|---|---|---|---|---|---|
| **Shaft** | 7850 | 0.5 | 0.3 | $210 \times 10^9$ | 0.0002 | 0 |
| | $\rho[\frac{kg}{m^3}]$ | $r[m]$ | $l[m]$ | | | |
| **Disks** | 7850 | 0.3 | 0.1 | | | |
| | $k_x[\frac{N}{m}]$ | $k_y[\frac{N}{m}]$ | $c_x[\frac{Ns}{m}]$ | $c_y[\frac{Ns}{m}]$ | | |
| **Bearings** | $1 \times 10^7$ | $1 \times 10^7$ | 100 | 100 | | |

dependence of the system on the spin speed $\Omega$. The inclusion of this parameter as a time dependent variable would make the solutions to the system much more difficult. In this work, the spin speed is considered to be constant in each operation taken in a series of operation as the value is changed. In this way, the effect of spin acceleration is not taken into account, but the dependence on spin speed is approximated. For the vast majority of rotordynamic systems this approximation is sufficiently accurate. For a simple critical speed computation without dependence on spin speed, $\Omega$, the homogeneous solution, using $\vec{\mathbf{q}} = e^{i\Omega t}$ while neglecting all damping and forcing, will provide the free whirling dynamic equation. In the case that the critical speeds need to be calculated with the inclusion of spin speed, like in the Campbell diagram, a solution of the form $\vec{\mathbf{q}}_0 e^{i\omega t}$ is used so that the spin speed and whirl speed can vary freely. Unbalance response is calculated using the particular integral as well.

Details of the different analyses to follow will be accompanied by an example problem to demonstrate the results. The problem of interest is a simple two disk rotor system depicted in Figure 1.8. The geometry and material properties are listed in Table 1.1. The Beam is discretized as in figure 1.8 with 6 elements. With geometry of $L = 1.8[m]$, $a = \frac{1}{3}L$, & $b = \frac{2}{3}L$ and bearing located at the ends of the shaft.

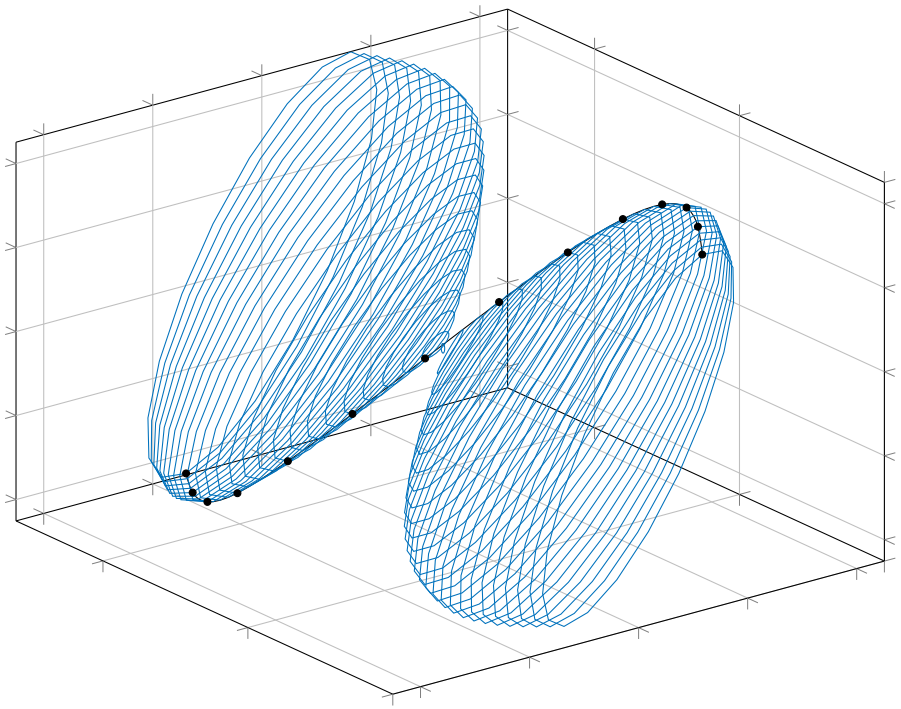

**Figure 1.8: Two disk rotor system used as an example.**

### 1.5.1 State Space Representation and the Eigenvalue Problem

The system can be represented in state space where,

$$\dot{\vec{\mathbf{z}}} = \underline{\mathbf{A}}\vec{\mathbf{z}} + \underline{\mathbf{B}}\vec{\mathbf{w}}, \quad \vec{\mathbf{z}} = \begin{Bmatrix} \dot{\vec{\mathbf{q}}} \\ \vec{\mathbf{q}} \end{Bmatrix} \tag{1.76}$$

$\underline{\mathbf{B}}\vec{\mathbf{w}}$ is an input into the system, which here will represent the forces due to unbalance. Solving for $\underline{\mathbf{A}}$ & $\underline{\mathbf{B}}\vec{\mathbf{w}}$

$$\underline{\mathbf{A}} = \begin{bmatrix} -\underline{\mathbf{M}}^{-1}\underline{\mathbf{D}} & -\underline{\mathbf{M}}^{-1}\underline{\mathbf{K}} \\ \underline{\mathbf{I}} & \underline{\mathbf{0}} \end{bmatrix} \quad \& \quad \underline{\mathbf{B}}\vec{\mathbf{w}} = \Omega^2 \begin{Bmatrix} \underline{\mathbf{M}}^{-1}\vec{\mathbf{F}} \\ 0 \end{Bmatrix} \tag{1.77}$$

This equation is valid in both the complex and real coordinate plane. With the use of complex coordinates, the state vector is represented by $\vec{\mathbf{z}} = [\dot{\vec{\mathbf{q}}}^c, \vec{\mathbf{q}}^c]^\intercal$. $\underline{\mathbf{I}}$ & $\underline{\mathbf{0}}$ are appropriately sized to match the matrices in the system of choice. $\underline{\mathbf{A}}$ is the dynamic matrix of the system, which represents the dynamics in a single expression. Now in

the form of a first order linear differential equation, numerical integration and many other numerical analysis techniques may be applied.

Using equation (1.76) and assuming a solution of $\vec{\mathbf{z}} = \vec{\mathbf{\Theta}} e^{st}$ leads to the eigenvalue problem

$$(\underline{\mathbf{A}} - s)\vec{\mathbf{\Theta}} = \underline{\mathbf{0}} \tag{1.78}$$

$\vec{\mathbf{\Theta}}$ is the vector containing the eigenvectors. Since the state in which these equations are defined is the combination of displacement and velocity, the eigenvectors are defined as a set corresponding to both displacement and velocity. This effectively duplicates the set as

$$\vec{\mathbf{\Theta}} = \left\{ \begin{array}{c} \vec{\theta}_{\dot{\vec{\mathbf{q}}}} \\ \vec{\theta}_{\vec{\mathbf{q}}} \end{array} \right\} = \left\{ \begin{array}{c} s\vec{\theta}_{\vec{\mathbf{q}}} \\ \vec{\theta}_{\vec{\mathbf{q}}} \end{array} \right\}$$

### 1.5.2 Unbalance Response

The unbalance response of the dynamic system can be achieved by substituting the particular integral $\vec{\mathbf{q}} = \vec{\mathbf{q}}_0 e^{i\Omega t}$ into the equation of motion (1.74),(1.75).

$$\vec{\mathbf{q}}_0 = (-\Omega^2 \underline{\mathbf{M}} + i\Omega \underline{\mathbf{D}} + \underline{\mathbf{K}})^{-1} \Omega^2 \vec{\mathbf{F}} \tag{1.79}$$

where the matrix in the parenthesis is called the dynamic response of the system. The dynamic response acts as a transfer matrix that converts inputs, $\vec{\mathbf{F}}$ into outputs $\vec{\mathbf{q}}_0$. The result is complex with the absolute part of the result representing the magnitude of the response, and the angle of the result as representing the phase delay of the response from the input. If the input phase is known in terms of shaft angle, then the phase delay of the response angle can be interpreted as a shaft angle.

The Unbalance response can also be calculated using the particular integral $\vec{\mathbf{q}} = \vec{\mathbf{q}}_0 e^{i\omega t}$ where $\omega$ is the independent whirl frequency. Then the response is found as the transfer response of the oscillation $e^{i(\Omega - \omega)t}$.

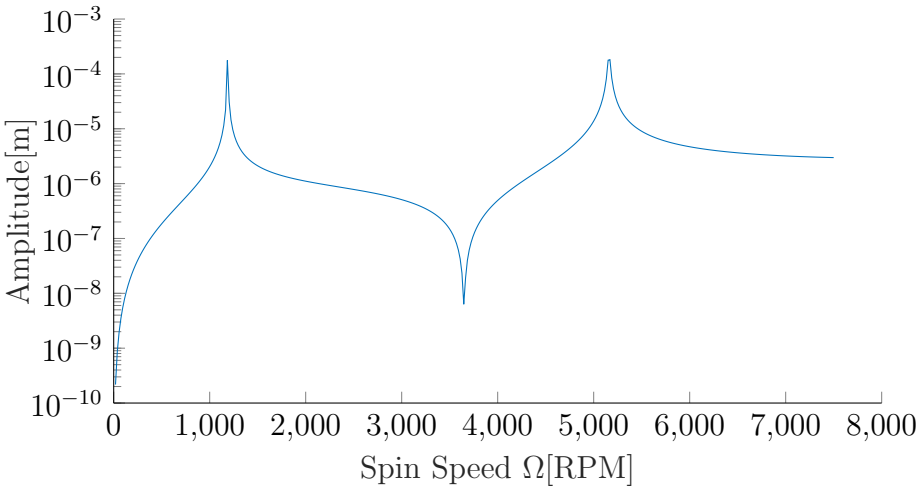


**Figure 1.9: Frequency response of the second disk subject to an unbalance at the second disk.**

For the example problem defined in §1.5 the unbalance response to a disk b unbalance of $2 \times 10^{-5}[m]$ is depicted in Figure **??**. We may enhance the frequency response figure by associating a plot of the phase angle with the response. This is called the Bode diagram and is presented in figure 1.10

### 1.5.3 Roots Locus and Stability Analysis

One of the most valuable facets of a rotordynamic model is its ability to predict instability. unstable operation can lead to rotor failures and unsafe operating conditions. Before the advent of modern mathematical models for rotating machinery, it was not common to operate a machine above the first critical speed. Internal damping and other rotating damping can cause a subsynchronous whirl when operating above the first critical speed. This effect is worse for machines with stiff bending modes, and is often instigated by loose fittings, shrink fits, and couplings. As mentioned in §1.1.2.6, the effect of external damping sources will not be investigated here. Rather, the stability will be tested by modeling the internal damping of the rotor due to viscous heat production during loading and unloading of the beam in bending. See §1.1.2.6

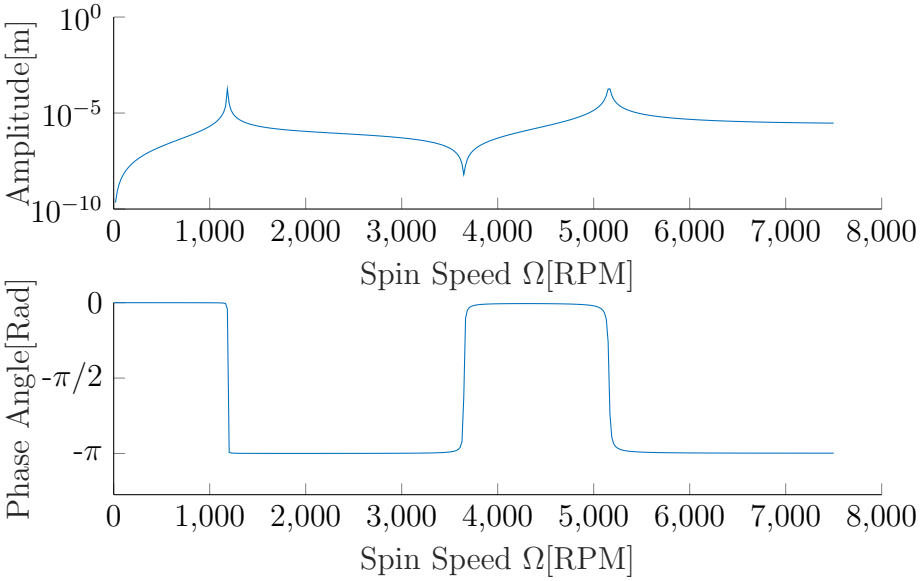


**Figure 1.10: Bode diagram of the second disk subject to an unbalance at the second disk.**

for a more detailed explanation and derivation.

Roots Locus is the plot of the eigenvalues on the $\Re - \Im$ plane as some value they are dependent on changes. In rotordynamic analysis the dependent variable is often the spin speed $\Omega$. In this plane, the eigenvalues $s$ represent the complex set of which the real part is the damping ans the imaginary is the damped natural frequency. The roots locus is useful in determining stability of the system, and which mode is responsible for the instability. Using the eigenvalues $s$ of the eigenvalue problem defined in equation (1.78) on the example problem defined in §1.5 a plot of the roots locus can be found as in figure 1.11. Internal damping coefficient, $\eta_v$, is added to the system at the value of $0.0002[s]$. The first three modes are presented with the negative complex couple joining each positive mode of vibration. In completely symmetric systems, the eigenvalue problem It is evident by looking at figure 1.11 that the system becomes unstable at some point, as many of the eigenvalues are in the positive real region of the plane. Since this example system is symmetric about the axis, the positive and negative pairs for each mode start at the same point when

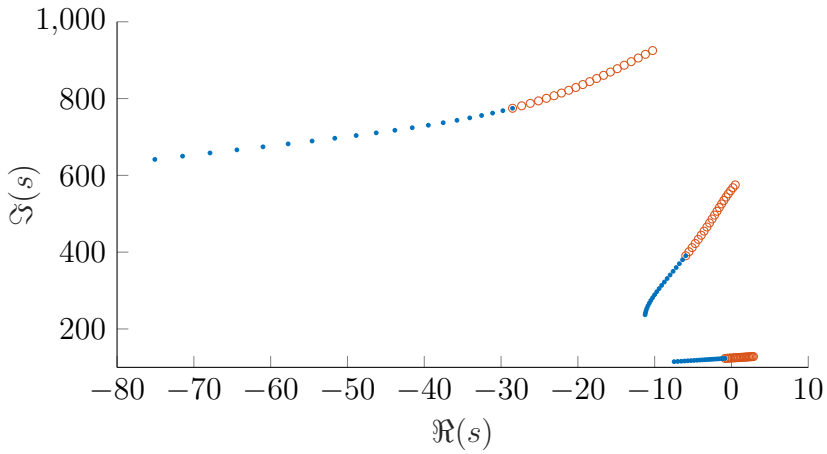


**Figure 1.11: Roots Locus of the example problem with an internal damping coefficient of 0.0002. Red circles represent positive frequencies, while blue dots represent negative ones.**

the spin speed is zero. The positive modes then move in the positive real direction–becoming more unstable. On the other hand, the negative frequencies move in the negative real direction–becoming more stable. This phenomena of the positive modes becoming more unstable and the negative becoming more stable is a general trend, but not a rule, and the rotating damping assists defined in §1.1.2.6 assists in this trend. Also, Gyroscopic effects tend to increase the whirl frequency (Imaginary part of eigenvalue) of the positive mode, while the opposite effect is seen in the negative mode.

The Roots Locus for the example problem is also presented in three dimensions to lend in the understanding of the relationship with spin speed. This can be seen in Figure 1.12. A direct method of measuring the stability of the system is to observe the real part of the eigenvalues of the dynamic matrix. Since the solution was assumed the be of the form $\vec{\mathbf{z}} = \vec{\mathbf{\Theta}} e^{st}$, then the eigenvalues represent the values of the complex exponent $s$. Splitting $s$ into its real and complex components as $s = \sigma + i\omega_d$, and plugging into $\vec{\mathbf{z}}$ gives: $\vec{\mathbf{z}} = \vec{\mathbf{\Theta}} e^{\sigma + i\omega_d}$. By inspection, it is evident that when the real part is positive, the response will grow without bound–an unstable system.

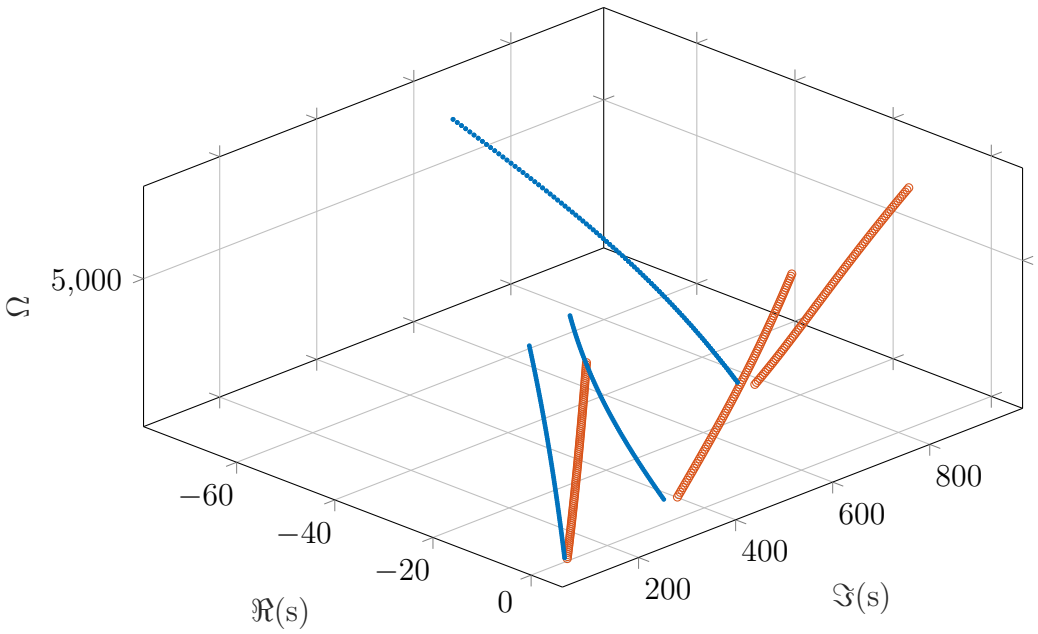


**Figure 1.12: Roots Locus of the example problem in 3-D with an internal damping coefficient of 0.0002. Red circles represent positive frequencies, while blue dots represent negative ones.**

Damping is Commonly represented as a the ratio of the real part of the eigenvalue to the natural frequency as

$$\zeta = \frac{-\sigma}{\omega_n} \ , \ \omega_n = \sqrt{\sigma^2 + \omega_d^2} \tag{1.80}$$

where $\zeta$ is the damping ratio, and $\omega_n$ is the natural frequency. The stability margin, or the range of speeds through which the system remains stable can be determined by plotting the maximum real part, $\Re(s)$, of the set against spin speed. The point at which $\Re(s)$, or $\sigma$, crosses the real axis is the threshold of stability. The plot which represents this is termed the Stability Margin plot, and is shown in 1.13 for the example problem defined in §1.5.

Finally, the stability can be analyzed using the damping coefficients($\zeta$) plotted against speed. This figure, shown in 1.14, indicates instability as when $\zeta$ drops below zero.

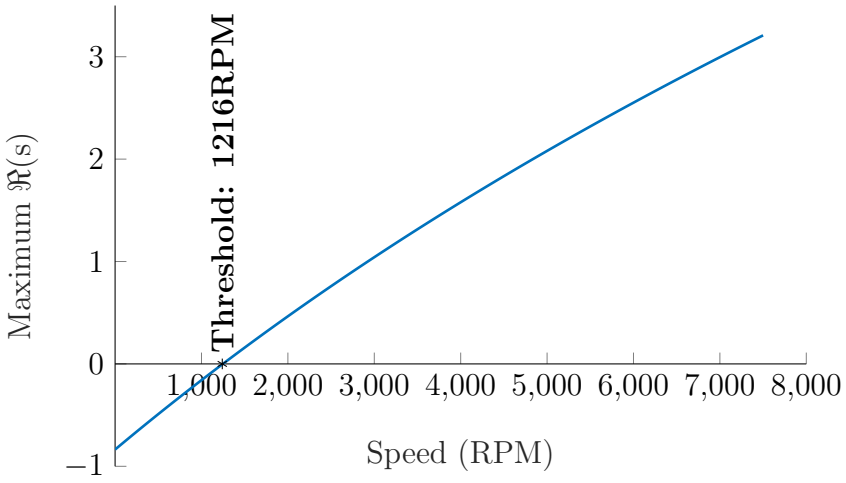


**Figure 1.13: length to radius ratio of 1.**

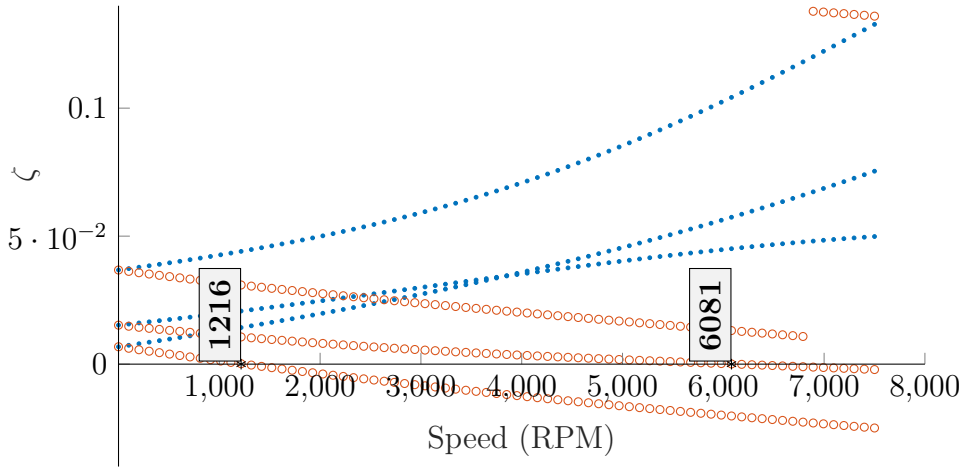


**Figure 1.14: Damping ratio vs. spin speed with indication of threshold of stability.**

### 1.5.4 Shapes

Deformed shape can be predicted using the eigenvectors of the eigenvalue problem 1.78. Eigenvectors contain displacement arrangement that corresponds to a natural frequency; this includes phase and relative amplitude of the generalized displacements from one another. For a simple model to conceptualize this idea, consider a rigid rod that can only translate in one plane at each end. The eigenvectors will contain all linearly independent combinations of the movement of the left side relative to the

right. This would be in general; opposite left to right (one up, one down), and same left and right(both up, or both down). The bending modes of the beam operate in a similar manner but scaled up, and just like in the simple case, including the same number of modes as there are degrees of freedom in the system. Since the state space representation used for eigenanalysis contains $\dot{\vec{\mathbf{q}}}$, & $\vec{\mathbf{q}}$ the eigenvector will contain $2N$ modes. For a general $i$th mode of vibration, the eigenvector $\vec{\mathbf{\Theta}}_i$ contains the displacement information. But, since the portion of $\vec{\mathbf{\Theta}}_i$ pertaining to velocities, $\vec{\theta}_{\dot{\vec{\mathbf{q}}}i}$, is a linear combination of $\vec{\theta}_{\vec{\mathbf{q}}i}$, all of the information is contained in one of these arrays. Therefore, the interpolation of displacements for the $i$th mode is given by

$$\vec{\mathbf{u}}_i = \underline{\mathbf{N}}\vec{\theta}_{\vec{\mathbf{q}}i} \tag{1.81}$$

where, the value of $\vec{\mathbf{u}}_i$ is now a function of $x$. So, through the choice of an array of positions that span the length of the beam element the displacement, and phase angle distribution of the $i$th mode of vibration is determined. Phase angle and amplitude of an transverse pair may be used to for an orbit of a beam axis location $x$.

Shape figures for the first 3 modes of the example problem are presented in Figures 1.15a,1.15b, and 1.15c. Note that the real and imaginary parts of the eigenvalues are listed along with the shapes. Also, note that the speed is chosen to coincide with the damped natural frequency so that this is the critical speed bending shape.

### 1.5.5 Campbell

The Campbell diagram correlates the spin speed and the whirl speed. The whirl speed is calculated as the imaginary part of the complex eigenvalue of the dynamic matrix (1.76). Spin speed is varied while calculating all of the critical speeds at each step of spin speed. The campbell diagram for the example problem is given in figure 1.16. This diagram can be used to discerne the critical speeds of the system. As can be seen in figure 1.16 the $\omega = \Omega$ synchronous line passes through 3 different complex modes

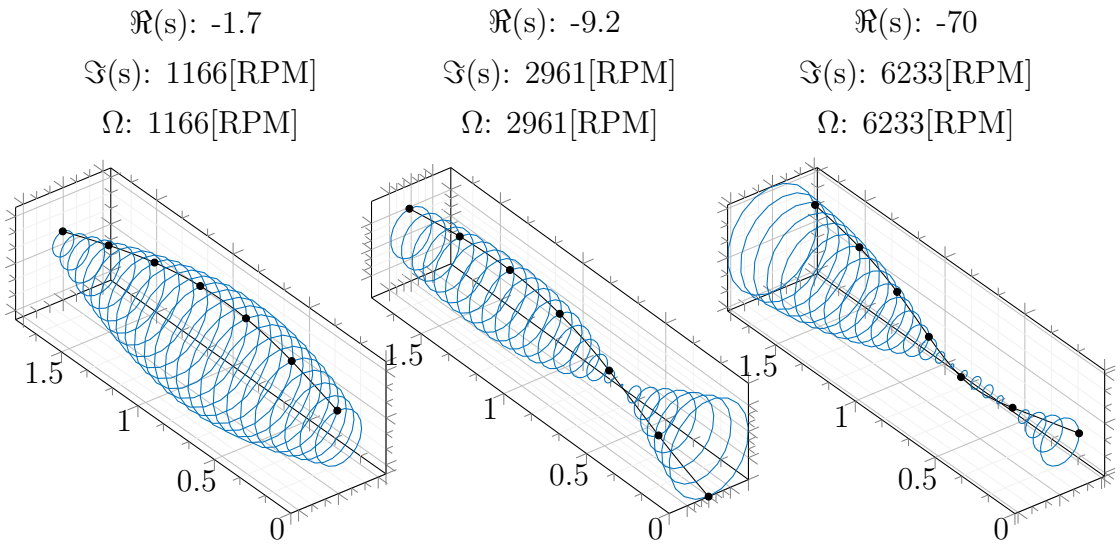


(a) Mode Shape 1. (b) Mode Shape 2. (c) Mode Shape 3.

**Figure 1.15: Modal shapes of the example problem.**

in this speed range. Note: with the large influence of the gyroscopic effect in the example problem presented here, the positive and negative frequencies for the second and third modes diverge from one another rath quickly. A physical interpretation of th selective effect of the gyroscopic moments can be presented by taking the mode shapes into account. Recall that the disks in the example are mounted at nodal locations 2 & 3. In figure 1.15 it is evident that in the first mode, Figure 1.15a, both disks are translating together. As a matter of fact, most of all the points of the system are translating in sync. This type of mode is called a cylindrical mode for the fact that as the whirl is traced, as it is in 1.15a, it forms a cylinder. The consequence of this type of motion is limiting on the transverse rotation angle of the mass elements. Since the gyroscopic moments are proportional to these angles, their magnitude is very low compared to transverse effects. On the contrary, in mode 2 & 3 pf figures 1.15b & 1.15c respectively, the angle of the disks and other mass elements is changing significantly through rotation. Because of this, large gyroscopic moments induce an out of phase force that stiffens positive whirl and softens negative whirl

tendencies. Gyroscopic moments are larger in these types of modes where there is a point of inflection on the beam, commonly called an antinode of vibration. This mode is called a conical mode, as analogous with the cylindrical mode, the shape of the path forms one or many cones.

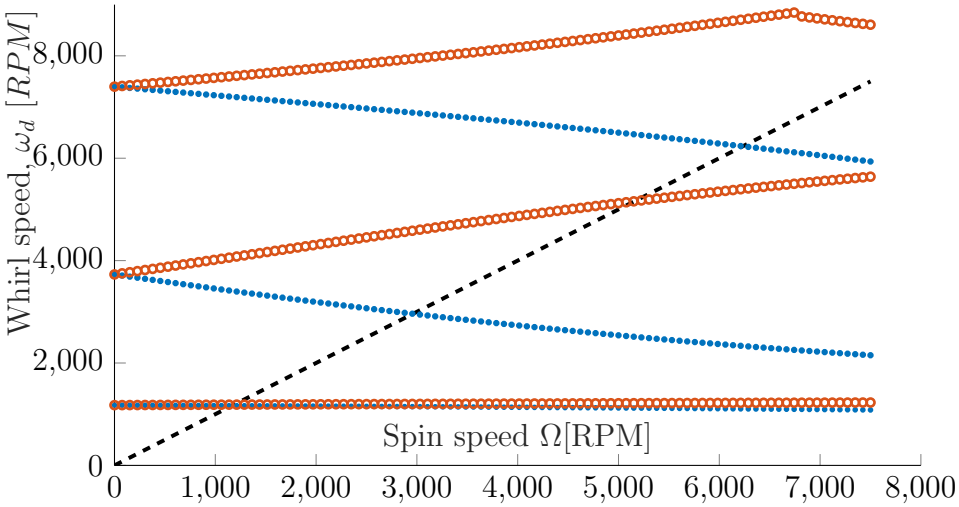


**Figure 1.16: Campbell Diagram of the example problem.**

# BIBLIOGRAPHY


[1] M. L. Adams. *Rotating machinery vibration: from analysis to troubleshooting*. CRC Press, 2009.

[2] L. Andersen and S. R. Nielsen. Elastic beams in three dimensions. *Aalborg University*, 2008.

[3] G. Barbaraci. Axial active magnetic bearing design. *Journal of Vibration and Control*, 22(5):1190–1197, 2016.

[4] D. E. Bently and T. Hatch'Charles. Fundamentals of rotating machinery diagnostics. *Mechanical Engineering-CIME*, 125(12):53–54, 2003.

[5] A. Bouaziz, S. Bouaziz, T. Hentati, J. Y. Cholley, and M. Haddar. Vibrations monitoring of high speed spindle with active magnetic bearings in presence of defects. *International Journal of Applied Electromagnetics and Mechanics*, 49(2):207–221, 2015.

[6] D. W. Childs. *Turbomachinery rotordynamics: phenomena, modeling, and analysis*. John Wiley & Sons, 1993.

[7] R. R. Craig and A. J. Kurdila. *Fundamentals of structural dynamics*. John Wiley & Sons, 2006.

[8] S. M. Darbandi, A. Habibollahi, M. Behzad, H. Salarieh, and H. Mehdigholi. Sensor runout compensation in active magnetic bearings via an integral adaptive observer. *Control Engineering Practice*, 48:111–118, 2016.

[9] A. Das, M. Nighil, J. Dutt, and H. Irretier. Vibration control and stability analysis of rotor-shaft system with electromagnetic exciters. *Mechanism and Machine Theory*, 43(10):1295–1316, 2008.

[10] A. Dimarogonas and S. Haddad. Vibration for engineers. *VhSˆ WI) IN914A R4 22k AWn 22kVAR5£ ilOuF 100k [ˆ. 2k 22k 22k*, page 252, 1993.

[11] B. Ertas and J. Vance. The influence of same-sign cross-coupled stiffness on rotordynamics. *Journal of Vibration and Acoustics*, 129(1):24–31, 2007.

[12] M. G. Farmakopoulos, M. D. Thanou, P. G. Nikolakopoulos, C. A. Papadopoulos, and A. P. Tzes. A control model of active magnetic bearings. In *Proceedings of the 3rd International Conference of Engineering Against Failure (ICEAF III)*, pages 26–28, 2013.

[13] L. Forrai. Stability analysis of symmetrical rotor-bearing systems with internal damping using finite element method. In *International Gas Turbine and AeroB engine Congress and Exhibition, Birmingham, UK*, 1996.

[14] G. Genta. Consistent matrices in rotor dynamic. *Meccanica*, 20(3):235–248, 1985.

[15] G. Genta. On a persistent misunderstanding of the role of hysteretic damping in rotordynamics. *TRANSACTIONS-AMERICAN SOCIETY OF MECHANICAL ENGINEERS JOURNAL OF VIBRATION AND ACOUSTICS*, 126(3):459–461, 2004.

[16] G. Genta. *Dynamics of rotating systems*. Springer Science & Business Media, 2007.

[17] T. Gmur and J. Rodrigues. Shaft finite elements for rotor dynamics analysis. *Journal of Vibration and Acoustics*, 113(4):482–493, 1991.

[18] U. Goerguelue. Beam theories the difference between euler-bernoulli and timoschenko. *Lecture Handouts*, 2009.

[19] P. Goldman and A. Muszynska. Application of full spectrum to rotating machinery diagnostics. *Orbit*, 20(1):17–21, 1999.

[20] N. Instruments. Ni labview for compactrio developer's guide. 2013.

[21] C. Jin, Y. Xu, J. Zhou, and C. Cheng. Active magnetic bearings stiffness and damping identification from frequency characteristics of control system. *Shock and Vibration*, 2016, 2016.

[22] M. A. Kandil. *On rotor internal damping instability*. PhD thesis, Imperial College London (University of London), 2005.

[23] B. Kirchgäßner. Finite elements in rotordynamics. *Procedia Engineering*, 144:736–750, 2016.

[24] A. Kuperman. Uncertainty and disturbance estimator-assisted control of a two-axis active magnetic bearing. *Transactions of the Institute of Measurement and Control*, 38(6):764–772, 2016.

[25] Y. Luo. An efficient 3d timoshenko beam element with consistent shape functions. *Adv. Theor. Appl. Mech*, 1(3):95–106, 2008.

[26] A. Muszynska. *Rotordynamics*. CRC press, 2005.

[27] V. Mykhaylyshyn. *Application of Active Magnetic Force Actuator for Control of Flexible Rotor System Vibrations*. PhD thesis, Cleveland State University, 2011.

[28] H. Nelson and J. McVaugh. The dynamics of rotor-bearing systems using finite elements. *Journal of Engineering for Industry*, 98(2):593–600, 1976.

[29] H. Roy, A. Das, and J. Dutt. An efficient rotor suspension with active magnetic bearings having viscoelastic control law. *Mechanism and Machine Theory*, 98:48–63, 2016.

[30] G. Schweitzer. Active magnetic bearings-chances and limitations. In *IFToMM Sixth International Conference on Rotor Dynamics, Sydney, Australia*, volume 1, pages 1–14, 2002.

[31] E. Swanson, C. D. Powell, and S. Weissman. A practical review of rotating machinery critical speeds and modes. *Sound and vibration*, 39(5):16–17, 2005.

[32] K. Tammi. *Active vibration control of rotor in desktop test environment*. VTT, 2003.

[33] J. M. Vance. *Rotordynamics of turbomachinery*. John Wiley & Sons, 1988.

[34] H. Wettergren and K.-O. Olsson. Dynamic instability of a rotating asymmetric shaft with internal viscous damping supported in anisotropic bearings. *Journal of sound and vibration*, 195(1):75–84, 1996.

[35] T. Yamamoto and Y. Ishida. *Linear and nonlinear rotordynamics: a modern treatment with applications*, volume 11. John Wiley & Sons, 2001.

[36] E. Zorzi and H. Nelson. Finite element simulation of rotor-bearing systems with internal damping. *Journal of Engineering for Power*, 99(1):71–76, 1977.